Focal drug administration via heparin-containing cryogel microcarriers reduces cancer growth and metastasis

Ben Newland[a,b]*, *Carmine Varricchio*[a], *Yvonne Körner*[b], *Franziska Hoppe*[b], *Christian Taplan*[b], *Heike Newland*[b], *Dimitri Eigel*[b], *Giusy Tornillo*[c], *Dagmar Pette*[b], *Andrea Brancale*[a], *Petra B. Welzel*[b], *F. Philipp Seib*[d,e], *Carsten Werner*[b,f]

[a] School of Pharmacy and Pharmaceutical Sciences, Cardiff University, King Edward VII Avenue, Cardiff, CF10 3NB, U.K. *Corresponding Author Email: newlandb@cardiff.ac.uk

[b] Leibniz-Institut für Polymerforschung Dresden, Max Bergmann Center of Biomaterials Dresden, Hohe Straße 6, D-01069 Dresden, Germany.

[c] European Cancer Stem Cell Research Institute, School of Biosciences, Hadyn Ellis Building, Cardiff University, Cardiff CF24 4HQ, U.K.

[d] Strathclyde Institute of Pharmacy and Biomedical Sciences, University of Strathclyde, 161 Cathedral Street, Glasgow, G4 0RE, U.K.

[e] EPSRC Future Manufacturing Research Hub for Continuous Manufacturing and Advanced Crystallisation (CMAC), University of Strathclyde, Technology and Innovation Centre, 99 George Street, Glasgow G1 1RD, U.K.

[f] Technische Universität Dresden, Center for Regenerative Therapies Dresden, Fetscherstr. 105, 01307 Dresden, Germany

Chemical compounds studied in this article:
Sodium heparin CID: 22833565
N-Ethyl-N′-(3-dimethylaminopropyl)carbodiimide (EDC) CID: 15908
N-Hydroxysulfosuccinimide (NHS) sodium salt CID: 133909
Dimethyl sulfoxide (DMSO) CID: 679
Toluene (≥99.5%) CID: 1140
Poly(ethylene glycol)-block-poly(propylene glycol)-block-poly(ethylene glycol) (Synperonic® PEP105) SID: 24888568
Alexa Fluor™ 647 CID: 102227060
Doxorubicin, hydrochloride salt CID: 443939

KEYWORDS: local drug delivery system, heparin, doxorubicin, sulfated microcarrier, cancer

ABSTRACT: Developing drug delivery systems that release anticancer drugs in a controlled and sustained manner remains challenging. We hypothesized that highly sulfated heparin-based microcarriers would allow electrostatic drug binding and controlled release. *In silico* modelling showed that the anticancer drug doxorubicin has affinity for the heparin component of the microcarriers. Experimental results showed that the strong electrostatic interaction was reversible, allowing both doxorubicin loading and a subsequent slow release over 42 days without an initial burst release. The drug-loaded microcarriers were able to reduce cancer cell viability *in vitro* in both hormone-dependent and highly aggressive triple-negative human breast cancer cells. Focal drug treatment, of an *in vivo* orthotopic triple-negative breast cancer model significantly decreased tumor burden and reduced cancer metastasis, whereas systemic administration of an equivalent drug dose was ineffective. This study proves that heparin-based microcarriers can be used as drug delivery platforms, for focal delivery and sustained long-term drug release.

1. Introduction

Chemotherapeutic drugs are a mainstay treatment for a wide variety of cancers, but the imprecise targeting of their toxic activity causes dose-limiting side effects. For example, adjuvant chemotherapies for breast cancer treatment are associated with severe long-term side effects, such as marrow neoplasms, premature menopause/infertility and cardiotoxicity (Tao, Visvanathan, & Wolff, 2015). Researchers are attempting to increase the local dose of these drugs at the tumor site by developing implantable drug delivery systems that can provide focal drug release when embedded within or in proximity to the tumor. These systems include, but are not limited to, hydrogels, scaffolds, microparticles and nanoparticles (Wolinsky, Colson, & Grinstaff, 2012). However, many of these drug delivery systems exhibit a "burst release" that delivers a disproportionately large amount of the drug immediately following implantation compared to later stages (Newland, Baeger, Eigel, Newland, & Werner, 2017; Newland et al., 2018; Pramod, Shah, & Jayakannan, 2015; Ying, Cui, Yu, & Du, 2011). Whilst this "burst" may be beneficial in certain therapeutic situations, it can be pharmacologically dangerous in others (i.e. it can produce unacceptable side effects), as well as being economically inefficient (Huang & Brazel, 2001). Ultimately, if the burst release is too pronounced, the drug can show a pharmacokinetic profile similar to that of systemic administration and produce similar adverse side effects. Better control over drug release remains a critical requirement, and this calls for drug release systems showing zero-order release kinetics, as well as self-regulating systems.

Long-term depot formulations are interesting contenders that could address this need (Yun, Lee, & Park, 2015). One interesting class of natural polymers for these formulations are the highly sulfated carbohydrates, such as heparin and heparan sulfate (Liang & Kiick, 2014). The abundance of sulfate groups (particularly in heparin) confers a highly negative charge on the polymer and facilitates the binding of a range of proteins (Rudd, Preston, & Yates, 2017).

Heparin-containing biomaterials have therefore been utilized for applications that require a slow and controlled release of heparin-binding proteins (Kang et al., 2019; K. Lee, Silva, & Mooney, 2011; Lohmann et al., 2017; Martino, Briquez, Maruyama, & Hubbell, 2015; Newland et al., 2015).

We hypothesized that the same process of electrostatic binding/slow release could be employed to design delivery devices for drugs that have positively charged moieties. One example is the chemotherapeutic drug doxorubicin, which is routinely used for breast cancer therapy (Hernandez-Aya & Gonzalez-Angulo, 2013) and which contains a primary amine that confers a positive charge under physiological conditions. Many researchers have exploited this amine group to generate covalent polymer-drug conjugates (Duncan & Vicent, 2010; Hervault et al., 2016; Pramod et al., 2015; Yoo, Oh, Lee, & Park, 1999). In the present study, we investigated whether a heparin-based system would allow reversible (electrostatic) binding of doxorubicin, while also affording sustained release over a period of one month.

We have previously prepared poly(ethylene glycol) (PEG)/heparin microscale scaffolds via cryogelation for cell transplantation applications (Newland et al., 2015). These spherical macroporous materials (termed microcarriers) are ideal for focal delivery because their compressible sponge-like structure allows their injection through fine-scale needles. Cryogels are clearly well-suited for cell delivery applications (Béduer et al., 2015; Bloch et al., 2005; Borg et al., 2016; Sarnowska et al., 2013),), but here we assessed their suitability as a focal drug delivery device. We analyzed whether these microcarriers can be loaded with doxorubicin, and whether the doxorubicin-loaded microcarriers can reduce breast cancer cell viability *in vitro*. We also evaluated whether locally administered doxorubicin-loaded microcarriers could serve as a viable therapeutic alternative to intravenously administered doxorubicin in an orthotopic metastatic breast cancer model.

2. Materials and Methods

2.1 Cryogel Microcarrier Synthesis and Characterization

Cryogel microcarriers were synthesized as described previously (Newland et al., 2020b). Briefly, 11.11 mg four-arm amino-terminated PEG (10 kDa, JenKem Technology, USA) was used to crosslink 15.56 mg heparin (14 kDa, sodium salt, porcine intestinal mucosa, Calbiochem, Merck, Germany) (1:1 molar ratio) via an EDC/sulfo-NHS mediated reaction (EDC = 1-ethyl-3-(3-dimethylaminopropyl)carbodiimide, 1.7 mg, Sigma, St. Louis, MO, USA; sulfo-NHS = N-hydroxysulfosuccinimide sodium salt, 0.97 mg, Sigma) in aqueous solution (600 µL of ice cold MilliQ water). A 1% (w/w) proportion of the heparin used in the cryogel microcarrier preparation was labelled with Alexa Fluor® 647 (Invitrogen, USA). The cryogel precursor solution was immediately added to a mixture of 9 mL toluene and 3 mL of the stabilizing agent poly(ethylene glycol)-block-poly(propylene glycol)-block-poly(ethylene glycol) (Synperonic PEP105, Sigma) in toluene solution (c = 1 mg/mL) in a round bottomed flask (stirring at 700 rpm). After 10 minutes another 3 mL of Synperonic PEP105 in toluene solution (1 mg/mL) was added before the round bottomed flask was submerged in an ethanol bath at -80 °C for 2 hours to initiate ice crystal formation in the water-in-toluene emulsion droplets. After storage at -20°C overnight, the toluene was carefully aspirated and the sample was lyophilized to remove the liquid phase of the hydrogel matrix.

The size distribution of the cryogel microcarriers was obtained by imaging 240 microcarriers in phosphate buffered saline (PBS) (Gibco, UK) using a brightfield light microscopy (10 × objective, Olympus IX73, Germany). Measurements were made using ImageJ software (NIH). Scanning electron microscopy (SEM, XL30 ESEM-FEG, Philips, Netherlands) was performed on dry microcarriers using the secondary electron detector and acceleration voltages of 3.0–5.0 kV. The samples were scattered on an SEM stub covered with

an adhesive carbon film and sputtered with gold for 60 s at 40 mA (SCD 050 Sputter Coater, Balzers) before imaging.

Fluorescence microscopy images of the cryogel microcarriers in PBS were obtained by confocal laser scanning microscopy (CLSM, Leica SP5, Leica, Germany) with a helium/neon laser (excitation wavelength 633 nm). Images were taken with a 10× magnification immersion objective (HCxPL APO CS 10×, aperture 0.4, IMM, Leica). Where z-plain stacks were taken, a z-distance between 2 and 5 μm was used.

Fourier-transform infrared spectroscopy was used as previously described (Eigel et al., 2019), to detect the heparin within the cryogel microcarriers.

2.2 In Silico Modelling of the Drug/Microcarrier Interaction

The computational studies were carried out using 1.80 GHz Intel Xeon (8 cores) processor-based computing, running Ubuntu 14.04 LTS. The model (a representative unit of the hydrogel structure) was prepared with Molecular Operating Environment 2015.10 (Sherbrooke St. W, Montreal, Canada). A representative unit of the cryogel polymer network was manually prepared using one molecule of PEG (10 kDa) and one molecule of heparin (14 kDa) to match the molar ratio used for the cryogel microcarrier synthesis (subsequently termed the "model PEG/heparin construct"). The three non-bound arms of the PEG chains were modelled as neutral amide groups; these were representative of the continuing network structure and thus did not contribute to charge-charge interactions In model #1, an Alexa Fluor® 647 molecule was also included in the structure to investigate the possible interactions of the drug with the fluorescent label (note that only 1% of the heparin was fluorescently labelled in the microcarriers). This fluorophore was omitted in model #2. The interaction of the drug (doxorubicin) with the model PEG/heparin construct was initially analyzed at a 1:1 molar ratio

(doxorubicin to heparin), and then at a 3:1 ratio to allow a closer representation of the drug loading ratio used in the experimental studies (i.e. the standard loading, see below).

Molecular dynamic simulations (Desmond package, Maestro v 11.4, Schrödinger LLC, New York, NY, 2017) were employed to identify the most stable conformation of the model PEG/heparin construct. Briefly, the model PEG/heparin construct was solvated with TIP3P water using an OPLS3 force field to form a water shell with a thickness of 20 Å around the model. The solvated model was then simulated with the "NPT relax protocol" in Desmond. That protocol involved an initial minimization of the solvent with restraints on the solute, followed by molecular dynamic simulations of 50 ns in NPT ensembles at constant temperature (300 K) and pressure (1 atm). Data were collected every 50 ps. The simulation was performed in triplicate, using a random seed as a starting point each time. Hierarchical clustering based on structural root-mean-squared distance (RMSD) was used to group the different polymer conformations and to select a representative structure for subsequent determination of drug interactions with the model PEG/heparin construct.

The molecular dynamic simulations of the drug-model interactions were performed using the "NPT relax protocol" in Desmond described above. The temperature of the simulations was taken as the default value of 300 K, and the duration of the simulation was 100 ns. Drug loading was determined by evaluating the variation of the total solute energy of the complex (drug + model PEG/heparin construct) with regards to the simulation time. The simulation was performed in triplicate, using a random seed as a starting point each time.

2.3 Doxorubicin Loading and Release Study

A 300 µL volume of doxorubicin solution was prepared by dissolving doxorubicin hydrochloride (LC Laboratories, Woburn, U.S.A) in dimethylsulphoxide (DMSO) and adding distilled water to give a DMSO concentration of 0.1% v/v. The doxorubicin was then added at

a concentration of either 400 µg/mL or 800 µg/mL to 1.8 mg of dry microcarriers. This resulted in either 66.6 µg doxorubicin per mg of microcarriers (MC) (dox/mg MC), termed "standard loading", or 133.3 µg dox/mg MC, termed "high loading". The molar ratio of doxorubicin to heparin was 2.76:1 (standard loading) or 5.52:1 (high loading). The microcarriers were left for 72 hours in the particular doxorubicin solution at room temperature. At the end of this loading period the supernatant was colorless and the microcarriers were dark red.

The loading and release characteristics were determined by removing supernatant samples after loading and at selected time points and storing them at -80°C for later analysis (see below). The removed volume was replaced with 900 µL of PBS (pH 7.4) (final microcarrier concentration of 2 mg/mL). The release was conducted at pH 7.4 in order to mimic the extracellular environment where the microcarriers were injected (proximal to the tumor), instead of the more acidic tumor microenvironment (Chen et al., 2015). At the end of the study (after 42 days), the collected supernatants were thawed and 100 µL were analyzed in a Spark® plate reader (Tecan Trading AG, Switzerland) by absorbance spectroscopy at 482 nm (concentrations above 1.5 µg/mL) and by fluorescence spectroscopy (concentrations below 1.5 µg/mL) at an excitation wavelength of 490 nm and emission wavelength of 595 nm. Standard curves were prepared for calculation of the released doxorubicin amounts, which were plotted as a cumulative release curve. The percentage of doxorubicin loaded onto the microcarriers was determined by a depletion method, i.e. by subtracting the doxorubicin concentration remaining in the supernatant after loading from its initial concentration in the loading solution. Experiments were performed in quadruplicate (n=4). The doxorubicin uptake by the microcarriers was visualised by CLSM, as described above, using an argon laser (excitation wavelength 488 nm) to image doxorubicin and a helium/neon laser (excitation wavelength 633 nm) to image the microcarriers.

2.4 Cell Viability Assays Comparing Unloaded and Doxorubicin Loaded Microcarriers

Two breast cancer cell lines were used for these studies. MCF-7 cells (ATCC, USA), were cultured in Dulbecco's Modified Eagle Medium (110 mg/L sodium pyruvate, 4.5 g/L glucose, Gibco/ThermoFisher) supplemented with 10% v/v fetal bovine serum (FBS, Biochrom, UK), 10 µg/mL insulin and penicillin (100 U/mL) and streptomycin (100 µg/mL) (Sigma). The metastatic breast cancer cell line MDA-MB-231 (ATCC) was cultured in Roswell Park Memorial Institute 1640 medium supplemented with 10% FBS and penicillin (100 U/mL) and streptomycin (100 µg/mL). Cells were seeded in a flat bottom 96-well plate at a density of 10,000 cells/well 24 h prior to experimentation. Microcarriers were loaded with doxorubicin at 40 µg dox/mg MC for 72 hours at 37°C. They were then washed three times with cell culture medium immediately prior to experimentation by allowing the microcarriers to sediment, removing the supernatant and replacing it with the appropriate cell culture medium. These loaded microcarriers were then diluted to 100 µg/mL. Unloaded microcarriers were suspended in the appropriate cell culture medium at a concentration of 100 µg/mL to serve as a control. Doxorubicin solution diluted to 4 µg/mL in cell culture medium was used as the positive control. The loaded microcarriers, unloaded microcarriers, and the positive control were incubated with the cells for 1 day and 3 days, prior to conducting light microscopy and PrestoBlue analysis. PrestoBlue (ThermoFisher, USA) was diluted to 10 % of its original concentration with cell culture medium and added to the cells for 30 minutes. Analysis was carried out according to the manufacturer's protocol with appropriate controls including a blank (no cells + PrestoBlue) and a microcarrier blank (no cells + microcarriers + PrestoBlue) to ensure no interaction of the materials with the assay. Experiments were performed in quadruplicate (n=4).

2.5 Analysis of Local Administration of Doxorubicin Loaded Microcarriers to an In Vivo Model of Metastatic Breast Cancer

The *in vivo* studies were approved by the Home Office of the United Kingdom (project license number PPL 70/8801). This study complied with best practice in cancer research (Workman et al., 2010), and all animals were maintained under Home Office regulations. The current *in vivo* trial was part of a multi-arm study to implement the principles of replacement, reduction and refinement (3Rs); therefore the control group and intravenous (i.v.) doxorubicin group were the same as described elsewhere.(Newland et al., 2018) MDA-MB-231-derived tumor cells were used to induce tumor xenografts that metastasized following orthotopic injection into mice; the tumors carried the firefly luciferase gene to permit *in vivo* bioluminescence imaging.(Goldstein, Reagan, Anderson, Kaplan, & Rosenblatt, 2010) Tumor formation, detection and therapeutic intervention were carried out based on protocols developed previously (Seib & Kaplan, 2012; Seib, Tsurkan, Freudenberg, Kaplan, & Werner, 2016). Briefly, female NOD/SCID mice (NOD.CB17-Prkd^{cscid}/NcrCrl) aged 49 to 56 days (Charles River UK Limited, UK) were injected bilaterally in the 4th or 5th mammary fat pad with a total of 5×10^5 cells in 20 µL of Matrigel (BD Biosciences, UK). Following tumor induction, the mice (group sizes 4 to 5) were treated on day 14.

Microcarriers (final concentration of 6 mg/mL) were loaded with doxorubicin at either 66.6 µg dox/mg MC (standard loading) or 133.3 µg dox/mg MC (high loading) for 72 hours before being drawn up into 1 mL syringes fitted with 26 gauge needles. Mice were injected bilaterally, close to the tumour sites, with 100 µL of microcarriers containing either a 40 µg "standard" or 80 µg "high" amount of doxorubicin. The mice therefore received a total of either 80 or 160 µg of doxorubicin per mouse. As a comparative control, the equivalent doxorubicin dose of 80 µg in normal saline was injected as a 100 µL bolus via the tail vein (denoted as "doxorubicin i.v."). This control was selected because it is the current primary

choice in the clinic. However, Abraxane® (nanoparticle albumin-bound paclitaxel), Myocet® (liposomal doxorubicin), Doxil® (PEGylated liposomal doxorubicin) are examples of clinically approved nanomedicine that are also administered intravenously (Venditto & Szoka Jr, 2013). Inclusion of one of these nanomedicines could have provided an interesting comparison, though freely diffusible doxorubicin in normal saline was considered the most appropriate benchmark. The control group received no treatments. Disease progression was monitored weekly by intraperitoneal injections of D-luciferin (Molecular Probes, Eugene USA) and measurement of tumour cell-associated bioluminescence using the Xenogen IVIS 200 imaging system. At the endpoint of the study, the bioluminescence imaging system was used to examine the brain, lung, liver and bones (hind legs) of each mouse for metastasis, and the primary tumours were dissected and weighed.

2.6 Statistical Analyses

GraphPad Prism 6.07 (GraphPad) software was used for data analysis. Tumor growth was analyzed using a two-way analysis of variance (ANOVA; treatment and time, repeated measures by treatment) with Tukey's post hoc multiple comparisons test. Tumor weight was analyzed by one-way ANOVA with Tukey's post hoc multiple comparisons test. Mouse total body and heart weights at the end of the study were also analyzed by one-way ANOVA with Tukey's post hoc multiple comparisons test. Error bars represent the standard deviation throughout, except for the *in vivo* analysis, where they represent the standard error of the mean. An asterisk denotes statistical significance as follows: *$P < 0.05$, **$P < 0.01$, ***$P < 0.001$.

3. Results and Discussion

3.1. Microcarrier Characterization

Heparin-containing cryogel microcarriers were formed from PEG and heparin using a previously established protocol (Newland et al., 2020a; Newland et al., 2020b) (Figure 1a, Supplementary Information (SI) Figure S1 and SI Figure S2). Scanning electron microscopy analysis showed the macroporous structure of the microcarriers in their dry state (Figure 1b). The addition of a small proportion of Alexa 647-labelled heparin during the synthesis procedure produced fluorescently labelled microcarriers that could be visualised in PBS (hydrated state) by confocal microscopy (Figure 1c). Analysis of the microcarrier size distribution (hydrated) (Figure 1d), showed that the microcarriers varied in diameter from 100 µm to 500 µm. The microcarriers had an average diameter of 232 µm (± 76 µm). The sponge-like nature of the cryogel materials allows their injection though needles far smaller than the microcarrier dimensions (Bencherif et al., 2012; Liu et al., 2014) as we have previously shown for these spherical microcarriers (Newland et al., 2015). This shape memory-like ability to re-expand after injection makes them an ideal material for focal delivery, where retention in the injection site is required.

3.2. *In Silico* Drug Loading: Doxorubicin Preferentially Binds to Heparin

The interactions between drugs and targets, or drugs and delivery systems, mainly depend on the structural, hydrophobic and electrostatic properties of both sets of molecules. These interactions are critical drivers for the formation of self-assembled supramolecular complexes. *In silico* studies can provide valuable insights into the forces involved in the formation of drug-carrier complexes and the possible drug-carrier interaction modes (Geetha, Sivaram, Jayakumar, & Gopi Mohan, 2016; Schirmer, Atallah, Werner, & Freudenberg, 2016). In the present study, molecular dynamic simulations were performed to predict the possible

interactions of doxorubicin with heparin-based microcarriers. As a first approach, a model was required that could represent the extended microcarrier system. Therefore, molecular dynamic simulations were performed using a PEG/heparin construct (25.8 kDa) as a model (Figure 2a). The root mean square deviation (RMSD) was then monitored throughout the simulation trajectories to determine the conformational changes of the model PEG/heparin construct and to identify the most stable structural conformation. This simulation showed an initial rearrangement of the polymer chains and a consecutive stabilization at an RMSD value around 16 Å (Figure 2b). This RMSD value was chosen as a cut-off for the selection of the different conformers, which were successively clustered to select a representative structure of the most stable polymer conformation of the model PEG/heparin construct (Figure 2c).

The doxorubicin loading was simulated using this representative model PEG/heparin construct structure (Figure 2c) as the model of the cryogel network. As a starting point, the drug was located close to the PEG region (Figure 3) and the drug-model PEG/heparin construct system was simulated for 50 ns using the NPT relax protocol. These molecular dynamic simulations showed a clear migration of doxorubicin from the PEG region of the model PEG/heparin construct to the heparin region through a pathway that involved a series of model-drug association and dissociation events (Figure 3, Supplementary Information Video S1).

The formation of the doxorubicin-heparin complex over time was then evaluated by analysing various parameters, such as RMSD, van der Waals energy, Coulomb's energy and total energy, throughout the simulation trajectory (SI Table S1). Analysis of the energy parameters of the molecular dynamic simulations revealed a considerable energetic change in the system over the simulation time; this change represented the stability of the drug-heparin complexes. The highest energy is usually representative of a more unfavorable situation, and consequently a less probable one, whereas a reduction in energy represents a favorable and more stable configuration. Here, the initial starting point of the doxorubicin-PEG interaction

showed a total system energy ranging from -3.65 to -28.11 kcal/mol, whereas the doxorubicin-heparin interaction energy was -22.1 to -40.9 kcal/mol. This energetic difference between the two complexes might explain the migration of doxorubicin from the PEG to the heparin region.

The affinity of doxorubicin for the heparin region has been further confirmed with a molecular dynamic simulation of 100 ns, using the same model PEG/heparin construct but with the starting point of doxorubicin at the heparin region of the construct (SI Figure S3). The results showed minimal RMSD variations and, overall, the lowest total energy, suggesting that the interaction between doxorubicin and the heparin region is the most favorable complex possible (SI Figure S3 and Video S2).

Another molecular dynamic simulation was performed using a molar ratio of doxorubicin to heparin of 3:1, as this more closely resembled the molar ratio used in the loading/release experiments and the *in vivo* studies (actual ratio 2.7:1). For this simulation, three starting locations were chosen for the doxorubicin molecules: the PEG region, the PEG/heparin border, and the heparin region. A simulation for 100 ns showed a migration of doxorubicin from the PEG region to the heparin region (Figure 4, SI Video S3). Further molecular dynamic simulations were carried out with a second model of PEG/heparin, but this time without a fluorophore (SI Figure S4). Doxorubicin again showed a preference for interacting with the heparin portion of the model, as shown in SI Figures S5 and S6.

In summary, *in silico* modelling showed that the heparin component of the cryogel microcarriers plays a crucial role in their drug loading capacity and is expected to directly impact the long and steady release of doxorubicin. These data are in accordance with previous studies showing doxorubicin binding to heparin or heparin hydrogels (Aoyama, Horioka, & Nagamitsu, 1987; Li, Ye, Zhang, & Feng, 2019; Wen et al., 2020; Yu et al., 2019). Here, the PEG region has only a marginal role in the doxorubicin-microcarrier interaction, suggesting

that specifically heparin-based microcarriers can be an efficient drug delivery platform for doxorubicin.

3.3. Heparin-Containing Microcarriers Load and Release Doxorubicin

Our initial hypothesis was that the sulfate groups on the heparin contained within the microcarriers would electrostatically attract doxorubicin via its amino group (proposed mechanism shown in SI Figure S7a). After confirmation of a doxorubicin-heparin interaction by *in silico* modelling, doxorubicin loading to the microcarriers was studied experimentally. Doxorubicin is red in color so we could clearly visualize the uptake process (Figure 5a and b).

Previously colorless microcarriers turned red after being left for 72 hours in a solution containing doxorubicin at a concentration of 800 μg/mL. Once washed (to remove unbound doxorubicin) the microcarriers stayed red whilst being observed in PBS using an optical microscope (Figure 5b). The doxorubicin appeared to be evenly distributed across the microcarrier, but a better visualization of the distribution was obtained with confocal fluorescence microscopy. The spectral separation of the doxorubicin and the AlexaFluor labeled microcarriers allowed the characterization of drug distribution on the microcarrier (Figure 5c). The overlay images of the drug loaded microcarrier appeared uniformly pink indicating that doxorubicin was bound evenly throughout the microcarriers. Doxorubicin was loaded at either 66.6 μg doxorubicin per mg of microcarrier (66.6 μg dox/mg MC) termed "standard loading" or 133.3 μg dox/mg MC termed "high loading". Regardless of the loading ratio used, all the doxorubicin in the solution was loaded onto the microcarriers (SI Figure S7b). Loading efficiencies (weight of drug/weight of microcarriers) of 6.6% and 13.3% were achieved for standard and high loadings, respectively. The molar ratio of doxorubicin loaded to heparin was calculated as 2.76 for standard loading and 5.52 for high loading (SI Figure S7c). Knowledge of the number of sulfate groups per mole of heparin (64.8) (assuming 24

disaccharide units for heparin, with 2.7 sulfate groups per unit) also allowed the calculation of the ratio of doxorubicin to sulfate groups, which was 0.043 for standard loading and 0.085 for high loading. Thus, a large excess of sulfate groups still remains at the loading concentrations used in these studies.

We then analyzed whether the heparin-containing microcarriers release doxorubicin in a sustained manner and without an uncontrolled burst release. Subsequent *in vivo* experiments analyzed microcarrier administration into the mammary fat pad rather than direct intratumoral injection, so PBS (pH 7.4) was used as a release medium. The supernatant surrounding doxorubicin-loaded microcarriers was analyzed over 42 days (the longest time tested). Approximately 25 µg of doxorubicin were released from the microcarriers over the first four days (Figure 5d), with the total release being 43 µg for standard loading and 52 µg for high loading. This release does not follow zero order kinetics, but no burst release of the drug occurred over the first two days and less than half the drug was released over the full 42 days (Figure 5e). Over the last three weeks, the microcarriers steadily released 1 to 2 µg of doxorubicin per week. At the end of the study ~50% (standard loading) or ~70% (high loading) of the drug still remained on the microcarriers (which still appeared dark red), indicating that doxorubicin that is tightly bound to the microcarriers either requires more time for release or competitive displacement via molecules with heparin-binding affinity which may occur in different mediums or the *in vivo* environment. We speculate that no significant chemical/physical changes to the microcarriers would be expected between PBS used for the release studies and culture medium (with similar salt content/pH) for the cytotoxicity analysis. However, serum components and proteins may serve to displace the doxorubicin, increasing the release rate (Shibata, Saito, Yomota, & Kawanishi, 2010). Furthermore, the release profile determined in PBS does not necessarily replicate the release situation *in vivo*, where

competitive ligands could adhere to doxorubicin (Agudelo et al., 2012), thus increasing the rate of doxorubicin displacement from the microcarriers.

Poly(lactic-co-glycolic acid)(PLGA) is commonly used to formulate microcarriers, microparticles and nanoparticles for applications in drug delivery (Davaa, Lee, Jenjob, & Yang, 2017; Kim et al., 2012, 2013; Pouponneau, Leroux, Soulez, Gaboury, & Martel, 2011). PLGA has tunable biodegradability and is a US Federal Drug Agency (FDA)-approved material for use in humans. However, several reports of PLGA-based doxorubicin delivery devices have shown rapid, short term release of doxorubicin (Kim et al., 2012, 2013; Pouponneau et al., 2011). For example, porous PLGA microparticles were shown to release their entire payload within 7 days (Kim et al., 2013) or 10 days (Kim et al., 2012). Another study showed that ~ 50% of the drug was released from PLGA microcarriers within the first 10 minutes (Pouponneau et al., 2011).

In these reports, the PLGA was used to physically encapsulate doxorubicin, so that release is possible via diffusion through the polymer network or via polymer degradation. The doxorubicin release time from PLGA microparticles has been greatly extended by covalently conjugating the doxorubicin to the microparticle via a peptide linker (Davaa et al., 2017). Multiple steps were required to create the microparticle-drug conjugates and although the release time was improved the release profile still showed a burst release during the first day. By contrast, our presented approach, which relies on the electrostatic binding of doxorubicin to the heparin-based microcarriers, allows a prolonged and steady release without a burst effect. This method of reversibly binding the doxorubicin to the microcarriers is both simple (no additional functionalization steps required) and effective.

3.4. Doxorubicin Loaded Microcarriers Reduce Breast Cancer Cell Viability *In Vitro*

Having ascertained that the microcarriers release the loaded doxorubicin in a sustained manner, we next analyzed whether the released payload could reduce the viability of human breast cancer cells. For these studies two tumorigenic human breast epithelial cell lines were chosen: MCF-7 cells with a non-invasive phenotype and MDA-MB-231 cells with an invasive phenotype (Castelló-Cros, Khan, Simons, Valianou, & Cukierman, 2009). Both MCF-7 and MDA-MB-231 cells were confirmed as sensitive to doxorubicin, as shown by the treatment with free doxorubicin at 4 µg/mL (positive control) in agreement with previous *in vitro* studies (Pilco-Ferreto & Calaf, 2016). Doxorubicin-loaded microcarriers showed a time-dependent cytotoxicity towards MCF-7 cells (Figure 6). Light microscopy analysis of the cells after 3 days of incubation (Figure 6c) showed that MCF-7 cells in the control group were growing in compact colonies with a polygonal morphology typical of differentiated breast cancer cells. However, treatment with doxorubicin (either as the free drug or through microcarrier release) caused shrinkage, rounding and detachment of the cells. The doxorubicin-loaded microcarriers caused a reduction in MCF-7 cell viability at a similar order of magnitude as the directly applied, freely diffusible doxorubicin.

The experimental setup also included MDA-MB-231 cells because they would be used to form the *in vivo* mouse metastatic breast cancer model. Again, administration of the doxorubicin loaded microcarriers resulted in a time-dependent cytotoxic effect (Figure 7). By day 3, microcarriers loaded with 40 µg dox/mg MC reduced the cell viability to 43%.

The unloaded microcarriers did not cause cytotoxicity towards MDA-MB-231 or MCF-7 cells. These data suggested that the microcarriers themselves are non-toxic, as expected from previous studies (Newland et al., 2015), but they can be used as a depot to deliver cytotoxic drugs like doxorubicin via injection.

3.5. Doxorubicin-loaded Microcarriers Reduce Tumor Growth, Tumor Weight and the Rate of Metastasis *In Vivo*

Despite improvements in breast cancer prognosis, triple-negative breast cancer remains a continuing clinical challenge with a high risk of tumor reoccurrence and poor outcomes. Triple-negative breast cancer comprises a heterogeneous group of tumors that are estrogen-receptor and progesterone-receptor negative and do not overexpress the human epidermal growth factor receptor 2 (HER2) (Bianchini, Balko, Mayer, Sanders, & Gianni, 2016). The lack of expression of these receptors renders triple-negative breast cancer unresponsive to anti-hormone or anti-HER2 therapy, leaving chemotherapy the only established drug-based therapeutic option (Denkert, Liedtke, Tutt, & von Minckwitz, 2017).

In the present study, the therapeutic efficiency of focal delivery of doxorubicin via locally injected microcarriers was compared to a bolus intravenous injection of doxorubicin. This required a model that would mimic the aggressive/challenging nature of triple-negative breast cancer. The orthotopic breast cancer mouse model was selected using bioluminescent triple-negative MDA-MB-231 cells, as this model shows a fast growth rate and exhibits a high rate of metastasis (Seib & Kaplan, 2012; Seib et al., 2016). The model also allows comparison of tumor growth rates and metastasis rates between focal and systemic drug administration.

The *in vivo* study included (i) no treatment (negative control), (ii) intravenous doxorubicin (positive control – 40 µg/tumor), (iii) doxorubicin-loaded microcarriers (standard loading – i.e. equivalent dose to positive control) and (iv) doxorubicin-loaded microcarriers (high loading – 80 µg/tumor) (Figure 8a). The dose of doxorubicin used for the intravenous injection (80 µg/mouse, i.e. 40 µg/tumor) was based on previous work that showed a significant decrease in tumor weight in this model but still had capacity for improvement (Seib & Kaplan, 2012). The microcarrier groups received the same mass of microcarriers, but these were loaded with different amounts of drug.

The rate of tumor growth, determined via bioluminescence analysis, was similar for all groups. The exception was the doxorubicin-loaded microcarrier (high loading) group, which showed an almost complete cessation of tumour growth (Figure 8b). This group showed a statistically significant difference from both the control group and the intravenous doxorubicin group ($P < .001$). This difference is apparent in the representative images of the bioluminescence analysis after six weeks (Figure 8c), as the images clearly show a smaller tumor-associated signal in comparison to the other groups.

At the end of the study, the tumor weight was lower for animals treated with intravenous doxorubicin than for the untreated control animals, although this difference did not reach statistical significance (Figure 8d). However, both doxorubicin-loaded–microcarrier groups (standard loading and high loading) showed a statistically significant reduction in the tumor burden ($P< .05$ and $P< .01$ respectively). The average tumor weight was 51 mg (± 48 mg) in the doxorubicin-loaded microcarrier group (high loading) and was significantly lower than the weights in both the no treatment control (549 mg ± 326 mg) and the intravenous doxorubicin group (414 mg ± 124 mg). Encouragingly, despite containing an equal dose of doxorubicin, the doxorubicin-loaded microcarrier group (standard loading) showed a greater reduction in tumor weight (290 mg ±189 mg) than was observed in the group of intravenously administered doxorubicin. These data prove the concept that focal delivery of doxorubicin can be as effective, or even more effective, than systemic administration. Furthermore, the slow nature of the drug release allows the delivery of a higher concentration locally to the tumor via the microcarriers, resulting in significantly reduced tumor growth and tumor burden. Polymer nanotubes, developed previously by our group, failed to achieve the level of controlled release of doxorubicin that was demonstrated by the heparin-based cryogel microcarriers (Newland et al., 2018). It should be noted that although heparin was incorporated into the microcarrier structure to control drug release, the interaction of free heparin with the tumor was not

investigated. Free heparin or nano-heparin derivatives have been reported to reduce cancer cell growth and metastasis (Afratis, Karamanou, Piperigkou, Vynios, & Theocharis, 2017). However, unloaded microcarriers caused no impact on MCF-7 or MDA-MB-231 breast cancer cells *in vitro*. We do not expect significant degradation of the microcarriers *in vitro* over the time periods tested minimizing free heparin shedding as microcarrier stocks show stability in PBS at room temperature for three years (data not shown). It is conceivable that the microcarriers could possibly be degraded *in vivo*, perhaps through macrophage activity. However, previous studies with PEG-crosslinked heparin (like that used herein) did not show any indication of degradation in the rat CNS after 21 days (Freudenberg et al., 2009).

Like other solid tumors, breast cancer tumors can metastasize and colonize other tissues. A study comparing the metastasis frequency and location of spread between triple-negative breast cancer and other breast cancer sub types revealed a higher rate of metastasis in triple-negative breast cancer (Dent et al., 2009). In our study, the use of bioluminescent cells allowed analysis of the spread to other tissues, such as brain, lung, liver and bone. All three doxorubicin treatments reduced metastasis rates (Figure 8e). This was particularly the case for bone, where all three doxorubicin groups showed lower rates than the untreated control. The brain had comparable metastasis rates across all groups and had lower metastasis rates than other organs.

In this triple-negative breast cancer mouse model, spread to the lungs is particularly prevalent (Newland et al., 2018; Seib & Kaplan, 2012), and was seen in 100% of all control animals. Doxorubicin loaded microcarriers reduced this lung metastasis rate to 75% (standard loading) or even 50% (high loading), confirming that focal delivery methods can outperform systemic drug administration techniques. At the high doxorubicin loading (dosing 7.2 mg/kg at an average mouse weight of 22 g) 1 out of 5 animals had to be euthanized due to ill health at 3.5 weeks. Nonetheless the microcarrier system allowed dose escalation well beyond a dose

typically tolerated in immune compromised animals (Favreau-Lessard, Blaszyk, Jones, Sawyer, & Pinz, 2019), without effecting mouse weight or heart weight (SI Figure S8).

Another advantage of the microcarriers developed here is the nature of their drug loading. Nanomaterials under development for drug delivery applications, by definition, have a high surface area to volume ratio, and this can be problematic for sustained delivery of the drug from the nanoparticle, especially when drug release is dependent on diffusion or degradation of the nanoparticle (J. H. Lee & Yeo, 2015). The microcarriers used in this study, with their macroporous structure, also have a high surface area to volume ratio, far larger than that of a non-porous microsphere of the same dimensions. However, no burst release of doxorubicin was observed (Figure 5). This indicates that using electrostatic attraction for loading drugs to a delivery system may be advantageous over more established techniques such as entrapment, encapsulation or covalent linking.

Previously developed heparin-based hydrogel aggregates also showed a controlled drug release profile, although that particular analysis was only carried out for four days (Seib et al., 2016). Herein we obtained a relatively steady release profile for 42 days with a maximum of 50% of the drug released during this period, despite complete replacement of the release medium at each time point (thus ensuring a maximum concentration gradient – i.e. "sink conditions"). The *in vivo* data also showed the feasibility of injecting doxorubicin-loaded microcarriers adjacent to the tumor site to result in a substantially greater reduction in tumor weight than the equivalent doxorubicin dose administered systemically. Furthermore, the drug dose could be doubled for delivery by the microcarriers to achieve an even more significant reduction in tumor growth.

4. Conclusion

In summary, cryogel microcarriers, composed of the sulfated polysaccharide heparin and poly(ethylene glycol), could load doxorubicin via simple electrostatic attraction of the drug

to the struts of the macroporous structure. *In silico* modelling highlighted the affinity of doxorubicin for the heparin component of the microcarriers. Sustained doxorubicin release was observed, without an initial burst, with approximately 50% of the doxorubicin released over 42 days (the longest time analyzed). Unloaded microcarriers did not cause cellular toxicity *in vitro*, corroborating previous studies showing that these microcarriers are non-toxic. However, cellular viability was reduced in the presence of doxorubicin-loaded microcarriers. Focal injection of doxorubicin-loaded microcarriers adjacent to an orthotopic breast cancer tumor in mice impeded both tumor growth and metastasis. These data indicate that biomaterials designed to incorporate sulphate groups through the use of natural carbohydrate polymers may represent an alternative and superior strategy for the focal and sustained release of positively charged drug molecules to solid tumors.

Appendix A. Supplementary data

Supplementary material related to this article can be found, in the online version

Author Information

Corresponding Author

*Email: newlandb@cardiff.ac.uk

Author Contributions

BN and FPS conceived the idea. CV and AB performed the molecular dynamic simulations. BN, YK, FH, CT, HN, DE and DP performed the materials synthesis and *in vitro* experiments, whilst FPS performed the *in vivo* analysis. GT, PBW and CW contributed to discussion and results analysis. BN wrote the manuscript with content edits by CT, FPS, PBW and CW.

Acknowledgments

BN would like to thank the Wellcome Trust for funding via a Sir Henry Wellcome Postdoctoral Fellowship and the Deutsche Forschungsgemeinschaft – Project number 320041273. The funding sources played no role in the experimental design or execution.

References

Afratis, N. A., Karamanou, K., Piperigkou, Z., Vynios, D. H., & Theocharis, A. D. (2017). The role of heparins and nano-heparins as therapeutic tool in breast cancer. *Glycoconjugate Journal,* 34(3), 299-307.

Agudelo, D., Bourassa, P., Bruneau, J., Berube, G., Asselin, É., & Tajmir-Riahi, H.-A. (2012). Probing the binding sites of antibiotic drugs doxorubicin and N-(trifluoroacetyl) doxorubicin with human and bovine serum albumins. *PLOS ONE,* 7(8).

Aoyama, T., Horioka, M., & Nagamitsu, S. (1987). Macromolecular complexes of drugs. I. Doxorubicin-heparin complex. *Chemical and Pharmaceutical Bulletin,* 35(2), 808-813.

Béduer, A., Braschler, T., Peric, O., Fantner, G. E., Mosser, S., Fraering, P. C., . . . Renaud, P. (2015). A compressible scaffold for minimally invasive delivery of large intact neuronal networks. *Advanced Healthcare Materials,* 4(2), 301-312.

Bencherif, S. A., Sands, R. W., Bhatta, D., Arany, P., Verbeke, C. S., Edwards, D. A., & Mooney, D. J. (2012). Injectable preformed scaffolds with shape-memory properties. *Proceedings of the National Academy of Sciences,* 109(48), 19590-19595.

Bianchini, G., Balko, J. M., Mayer, I. A., Sanders, M. E., & Gianni, L. (2016). Triple-negative breast cancer: challenges and opportunities of a heterogeneous disease. *Nature Reviews Clinical Oncology,* 13(11), 674.

Bloch, K., Lozinsky, V. I., Galaev, I. Y., Yavriyanz, K., Vorobeychik, M., Azarov, D., . . . Vardi, P. (2005). Functional activity of insulinoma cells (INS-1E) and pancreatic islets cultured in agarose cryogel sponges. *Journal of Biomedical Materials Research Part A,* 75A(4), 802-809.

Borg, D. J., Welzel, P. B., Grimmer, M., Friedrichs, J., Weigelt, M., Wilhelm, C., . . . Werner, C. (2016). Macroporous biohybrid cryogels for co-housing pancreatic islets with mesenchymal stromal cells. *Acta Biomaterialia,* 44, 178-187.

Castelló-Cros, R., Khan, D. R., Simons, J., Valianou, M., & Cukierman, E. (2009). Staged stromal extracellular 3D matrices differentially regulate breast cancer cell responses through PI3K and beta1-integrins. *BMC Cancer,* 9(1), 94.

Chen, L. Q., Randtke, E. A., Jones, K. M., Moon, B. F., Howison, C. M., & Pagel, M. D. (2015). Evaluations of tumor acidosis within in vivo tumor models using parametric maps generated with acidoCEST MRI. *Molecular Imaging and Biology,* 17(4), 488-496.

Davaa, E., Lee, J., Jenjob, R., & Yang, S.-G. (2017). MT1-MMP responsive doxorubicin conjugated poly(lactic-co-glycolic acid)/poly(styrene-alt-maleic anhydride) core/shell microparticles for intrahepatic arterial chemotherapy of hepatic cancer. *ACS Applied Materials & Interfaces,* 9(1), 71-79.

Denkert, C., Liedtke, C., Tutt, A., & von Minckwitz, G. (2017). Molecular alterations in triple-negative breast cancer—the road to new treatment strategies. *The Lancet,* 389(10087), 2430-2442.

Dent, R., Hanna, W. M., Trudeau, M., Rawlinson, E., Sun, P., & Narod, S. A. (2009). Pattern of metastatic spread in triple-negative breast cancer. *Breast Cancer Research and Treatment,* 115(2), 423-428.

Duncan, R., & Vicent, M. J. (2010). Do HPMA copolymer conjugates have a future as clinically useful nanomedicines? A critical overview of current status and future opportunities. *Advanced Drug Delivery Reviews,* 62(2), 272-282.

Eigel, D., Zoupi, L., Sekizar, S., Welzel, P. B., Werner, C., Williams, A., & Newland, B. (2019). Cryogel scaffolds for regionally constrained delivery of lysophosphatidylcholine to central nervous system slice cultures: A model of focal demyelination for multiple sclerosis research. *Acta Biomaterialia,* 97, 216.

Favreau-Lessard, A. J., Blaszyk, H., Jones, M. A., Sawyer, D. B., & Pinz, I. M. (2019). Systemic and cardiac susceptibility of immune compromised mice to doxorubicin. *Cardio-Oncology,* 5(1), 2.

Freudenberg, U., Hermann, A., Welzel, P. B., Stirl, K., Schwarz, S. C., Grimmer, M., . . . Werner, C. (2009). A star-PEG–heparin hydrogel platform to aid cell replacement therapies for neurodegenerative diseases. *Biomaterials,* 30(28), 5049-5060.

Geetha, P., Sivaram, A. J., Jayakumar, R., & Gopi Mohan, C. (2016). Integration of in silico modeling, prediction by binding energy and experimental approach to study the amorphous chitin nanocarriers for cancer drug delivery. *Carbohydrate Polymers,* 142, 240-249.

Goldstein, R. H., Reagan, M. R., Anderson, K., Kaplan, D. L., & Rosenblatt, M. (2010). Human bone marrow–derived MSCs can home to orthotopic breast cancer tumors and promote bone metastasis. *Cancer Research,* 70(24), 10044-10050.

Hernandez-Aya, L. F., & Gonzalez-Angulo, A. M. (2013). Adjuvant systemic therapies in breast cancer. *Surgical Clinics,* 93(2), 473-491.

Hervault, A., Dunn, A. E., Lim, M., Boyer, C., Mott, D., Maenosono, S., & Thanh, N. T. K. (2016). Doxorubicin loaded dual pH- and thermo-responsive magnetic nanocarrier for combined magnetic hyperthermia and targeted controlled drug delivery applications. *Nanoscale,* 8(24), 12152-12161.

Huang, X., & Brazel, C. S. (2001). On the importance and mechanisms of burst release in matrix-controlled drug delivery systems. *Journal of Controlled Release,* 73(2), 121-136.

Kang, S., Yoon, J. S., Lee, J. Y., Kim, H.-J., Park, K., & Kim, S. E. (2019). Long-term local PDGF delivery using porous microspheres modified with heparin for tendon healing of rotator cuff tendinitis in a rabbit model. *Carbohydrate Polymers,* 209, 372-381.

Kim, I., Byeon, H. J., Kim, T. H., Lee, E. S., Oh, K. T., Shin, B. S., . . . Youn, Y. S. (2012). Doxorubicin-loaded highly porous large PLGA microparticles as a sustained-release inhalation system for the treatment of metastatic lung cancer. *Biomaterials,* 33(22), 5574-5583.

Kim, I., Byeon, H. J., Kim, T. H., Lee, E. S., Oh, K. T., Shin, B. S., . . . Youn, Y. S. (2013). Doxorubicin-loaded porous PLGA microparticles with surface attached TRAIL for the inhalation treatment of metastatic lung cancer. *Biomaterials,* 34(27), 6444-6453.

Lee, J. H., & Yeo, Y. (2015). Controlled drug release from pharmaceutical nanocarriers. *Chemical Engineering Science,* 125, 75-84.

Lee, K., Silva, E. A., & Mooney, D. J. (2011). Growth factor delivery-based tissue engineering: general approaches and a review of recent developments. *Journal of The Royal Society Interface,* 8(55), 153.

Li, Q., Ye, L., Zhang, A., & Feng, Z. (2019). The preparation and morphology control of heparin-based pH sensitive polyion complexes and their application as drug carriers. *Carbohydrate Polymers,* 211, 370-379.

Liang, Y., & Kiick, K. L. (2014). Heparin-functionalized polymeric biomaterials in tissue engineering and drug delivery applications. *Acta Biomaterialia,* 10(4), 1588-1600.
Liu, W., Li, Y., Zeng, Y., Zhang, X., Wang, J., Xie, L., . . . Du, Y. (2014). Microcryogels as injectable 3-D cellular microniches for site-directed and augmented cell delivery. *Acta Biomaterialia,* 10(5), 1864-1875.
Lohmann, N., Schirmer, L., Atallah, P., Wandel, E., Ferrer, R. A., Werner, C., . . . Freudenberg, U. (2017). Glycosaminoglycan-based hydrogels capture inflammatory chemokines and rescue defective wound healing in mice. *Science Translational Medicine,* 9(386).
Martino, M. M., Briquez, P. S., Maruyama, K., & Hubbell, J. A. (2015). Extracellular matrix-inspired growth factor delivery systems for bone regeneration. *Advanced Drug Delivery Reviews,* 94, 41-52.
Newland, B., Baeger, M., Eigel, D., Newland, H., & Werner, C. (2017). Oxygen-producing gellan gum hydrogels for dual delivery of either oxygen or peroxide with doxorubicin. *ACS Biomaterials Science & Engineering,* 3(5), 787-792.
Newland, B., Ehret, F., Hoppe, F., Eigel, D., Pette, D., Newland, H., . . . Werner, C. (2020a). Macroporous heparin-based microcarriers allow long-term 3D culture and differentiation of neural precursor cells *Biomaterials,* 230, 119540.
Newland, B., Ehret, F., Hoppe, F., Eigel, D., Pette, D., Newland, H., . . . Werner, C. (2020b). Static and dynamic 3D culture of neural precursor cells on macroporous cryogel microcarriers. *MethodsX,* 7, 100805.
Newland, B., Taplan, C., Pette, D., Friedrichs, J., Steinhart, M., Wang, W., . . . Werner, C. (2018). Soft and flexible poly(ethylene glycol) nanotubes for local drug delivery. *Nanoscale,* 10(18), 8413-8421.
Newland, B., Welzel, P. B., Newland, H., Renneberg, C., Kolar, P., Tsurkan, M., . . . Werner, C. (2015). Tackling cell transplantation anoikis: An injectable, shape memory cryogel microcarrier platform material for stem cell and neuronal cell growth. *Small,* 11(38), 5047-5053.
Pilco-Ferreto, N., & Calaf, G. M. (2016). Influence of doxorubicin on apoptosis and oxidative stress in breast cancer cell lines. *International Journal of Oncology,* 49(2), 753-762.
Pouponneau, P., Leroux, J.-C., Soulez, G., Gaboury, L., & Martel, S. (2011). Co-encapsulation of magnetic nanoparticles and doxorubicin into biodegradable microcarriers for deep tissue targeting by vascular MRI navigation. *Biomaterials,* 32(13), 3481-3486.
Pramod, P. S., Shah, R., & Jayakannan, M. (2015). Dual stimuli polysaccharide nanovesicles for conjugated and physically loaded doxorubicin delivery in breast cancer cells. *Nanoscale,* 7(15), 6636-6652.
Rudd, T. R., Preston, M. D., & Yates, E. A. (2017). The nature of the conserved basic amino acid sequences found among 437 heparin binding proteins determined by network analysis. *Molecular BioSystems,* 13(5), 852-865.
Sarnowska, A., Jablonska, A., Jurga, M., Dainiak, M., Strojek, L., Drela, K., . . . Jungvid, H. (2013). Encapsulation of mesenchymal stem cells by bioscaffolds protects cell survival and attenuates neuroinflammatory reaction in injured brain tissue after transplantation. *Cell Transplantation,* 22(1), S67-S82.
Schirmer, L., Atallah, P., Werner, C., & Freudenberg, U. (2016). StarPEG-heparin hydrogels to protect and sustainably deliver IL-4. *Advanced Healthcare Materials,* 5(24), 3157-3164.
Seib, F. P., & Kaplan, D. L. (2012). Doxorubicin-loaded silk films: Drug-silk interactions and in vivo performance in human orthotopic breast cancer. *Biomaterials,* 33(33), 8442-8450.

Seib, F. P., Tsurkan, M., Freudenberg, U., Kaplan, D. L., & Werner, C. (2016). Heparin-modified polyethylene glycol microparticle aggregates for focal cancer chemotherapy. *ACS Biomaterials Science & Engineering,* 2(12), 2287-2293.

Shibata, H., Saito, H., Yomota, C., & Kawanishi, T. (2010). Ammonium ion level in serum affects doxorubicin release from liposomes. *Die Pharmazie-An International Journal of Pharmaceutical Sciences,* 65(4), 251-253.

Tao, J. J., Visvanathan, K., & Wolff, A. C. (2015). Long term side effects of adjuvant chemotherapy in patients with early breast cancer. *The Breast,* 24, S149-S153.

Venditto, V. J., & Szoka Jr, F. C. (2013). Cancer nanomedicines: so many papers and so few drugs! *Advanced Drug Delivery Reviews,* 65(1), 80-88.

Wen, J., Chen, Q., Ye, L., Zhang, H., Zhang, A., & Feng, Z. (2020). The preparation of pH and GSH dual responsive thiolated heparin/DOX complex and its application as drug carrier. *Carbohydrate Polymers,* 230, 115592.

Wolinsky, J. B., Colson, Y. L., & Grinstaff, M. W. (2012). Local drug delivery strategies for cancer treatment: Gels, nanoparticles, polymeric films, rods, and wafers. *Journal of Controlled Release,* 159(1), 14-26.

Workman, P., Aboagye, E., Balkwill, F., Balmain, A., Bruder, G., Chaplin, D., . . . Glennie, M. (2010). Guidelines for the welfare and use of animals in cancer research. *British Journal of Cancer,* 102(11), 1555.

Ying, X.-Y., Cui, D., Yu, L., & Du, Y.-Z. (2011). Solid lipid nanoparticles modified with chitosan oligosaccharides for the controlled release of doxorubicin. *Carbohydrate Polymers,* 84(4), 1357-1364.

Yoo, H. S., Oh, J. E., Lee, K. H., & Park, T. G. (1999). Biodegradable nanoparticles containing doxorubicin-PLGA conjugate for sustained release. *Pharmaceutical Research,* 16(7), 1114-1118.

Yu, Y., Xu, C., Zhen, L., Yang, S., Zhou, J., & Yao, J. (2019). Bio-inspired drug-dominated supramolecular nanocomplex based on low molecular weight heparin for progressive tumor therapy. *Carbohydrate Polymers,* 220, 30-42.

Yun, Y. H., Lee, B. K., & Park, K. (2015). Controlled drug delivery: historical perspective for the next generation. *Journal of Controlled Release,* 219, 2-7.

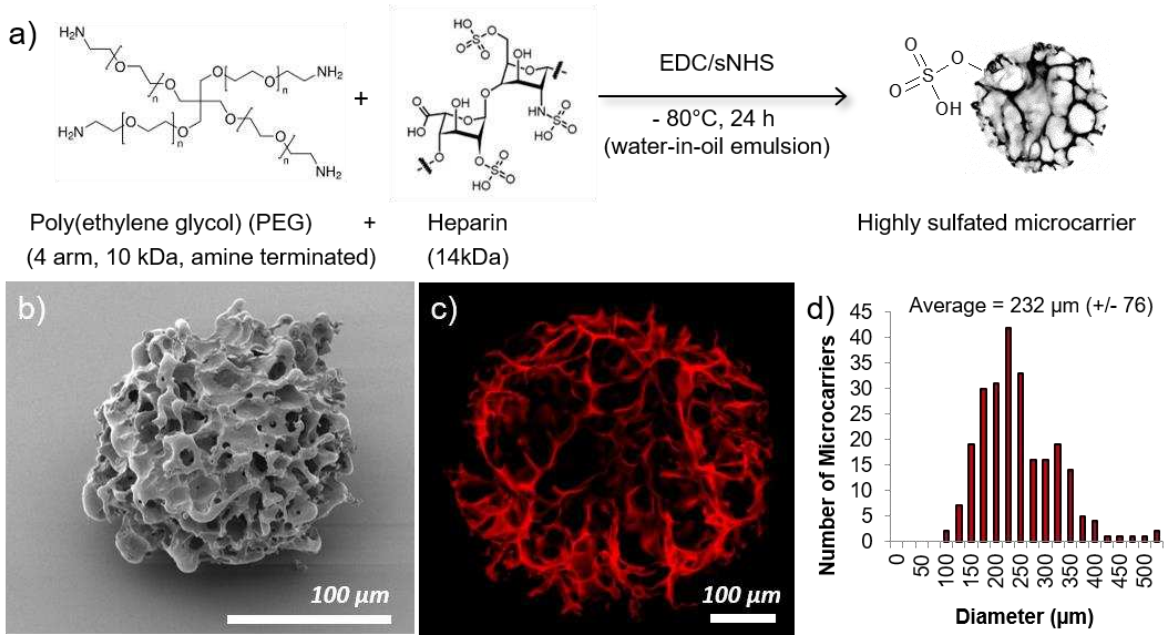

Figure 1. Sulfated cryogel microcarriers synthesized from poly(ethylene glycol) (PEG) and heparin. (a) A schematic depiction of the cryogel synthesis procedure (mechanism shown in SI Figure S1). (b) A scanning electron microscope image of a microcarrier under vacuum showing the macroporous structure. (c) Alexa 647 labeling of the microcarriers allows confocal laser fluorescence microscopy analysis in their swollen state (PBS). (d) Size distribution analysis of 244 microcarriers in their PBS swollen state, showing an average diameter of 232 ± 76 µm.

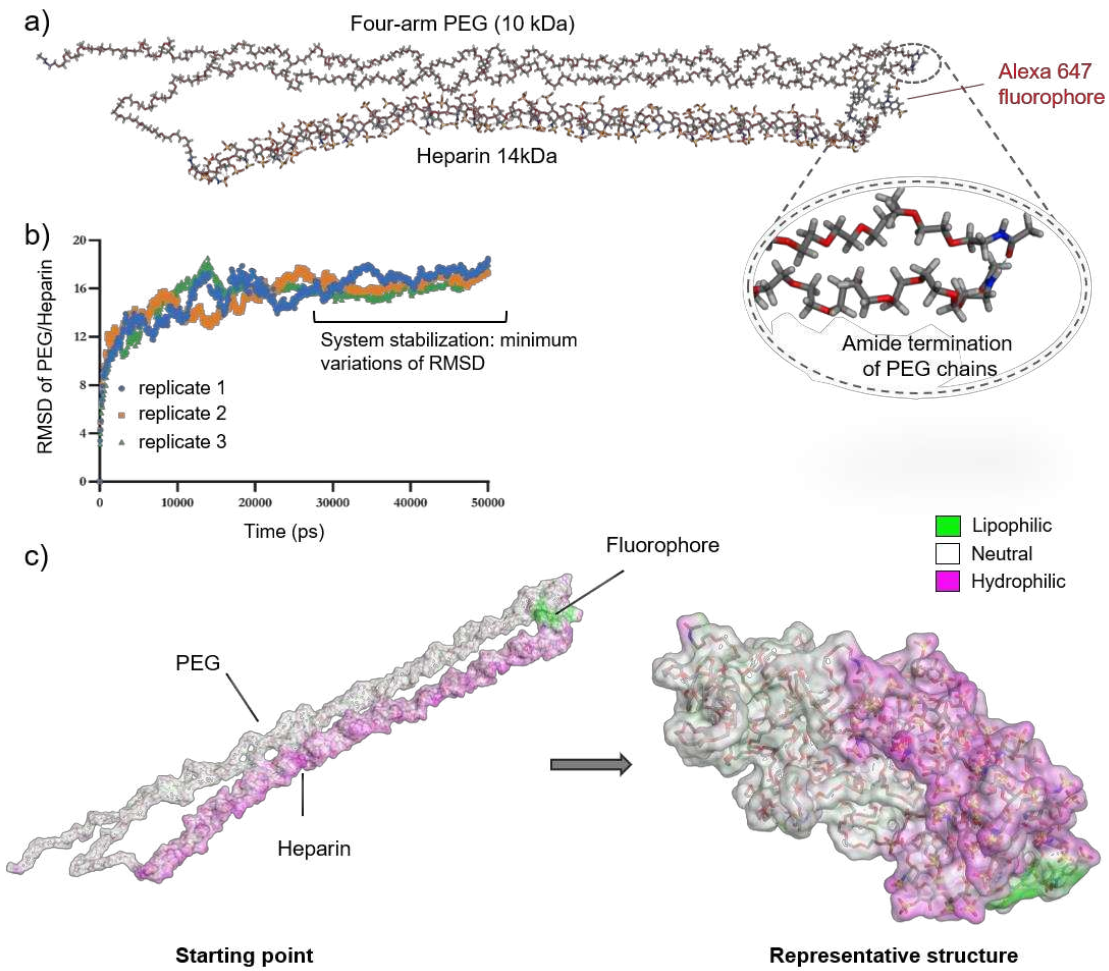

Figure 2. A model PEG/heparin construct that represents a unit of the hydrogel structure for molecular dynamic simulations: (a) Molecular structure of the model PEG/heparin construct created from one PEG molecule and one heparin molecule (i.e. the same molar ratio as used for microcarrier preparation) plus an Alexa fluorophore. (b) Graph showing the root-mean-squared distance (RMSD) vs time for the model PEG/heparin construct in water (n=3), from which the representative folded structure (used for subsequent computational analyses) was derived; this structure is rendered in (c).

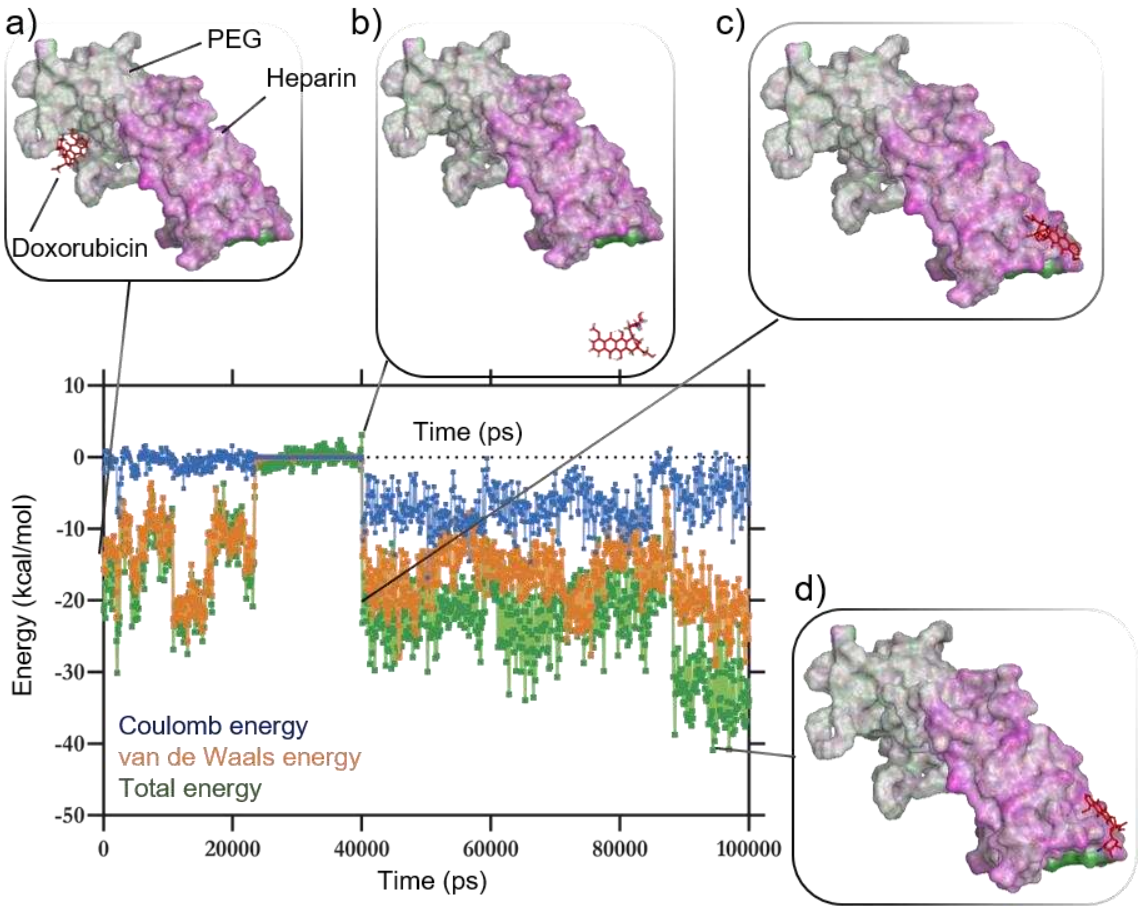

Figure 3. Molecular dynamic simulation of the interaction of doxorubicin with the model PEG/heparin construct clearly shows the preferential binding of doxorubicin to the heparin region rather than to the PEG region of the construct. The graph shows the variations of energy (Coulomb – blue, van de Waals – orange, and total energy – green) of the system during the simulation (system contains one doxorubicin molecule and one model PEG/heparin construct). The four images show the molecular structures in different states of the system during the simulation. (a) The position and orientation of doxorubicin at time 0 (i.e. starting point) when placed near the PEG region of the model construct. (b) The doxorubicin position when the total energy is the highest (i.e. in the surrounding water). (c) The initial interaction of doxorubicin with the heparin part of the model PEG/heparin construct and (d) in the most stable condition) (see supplementary video S1 for full simulation).

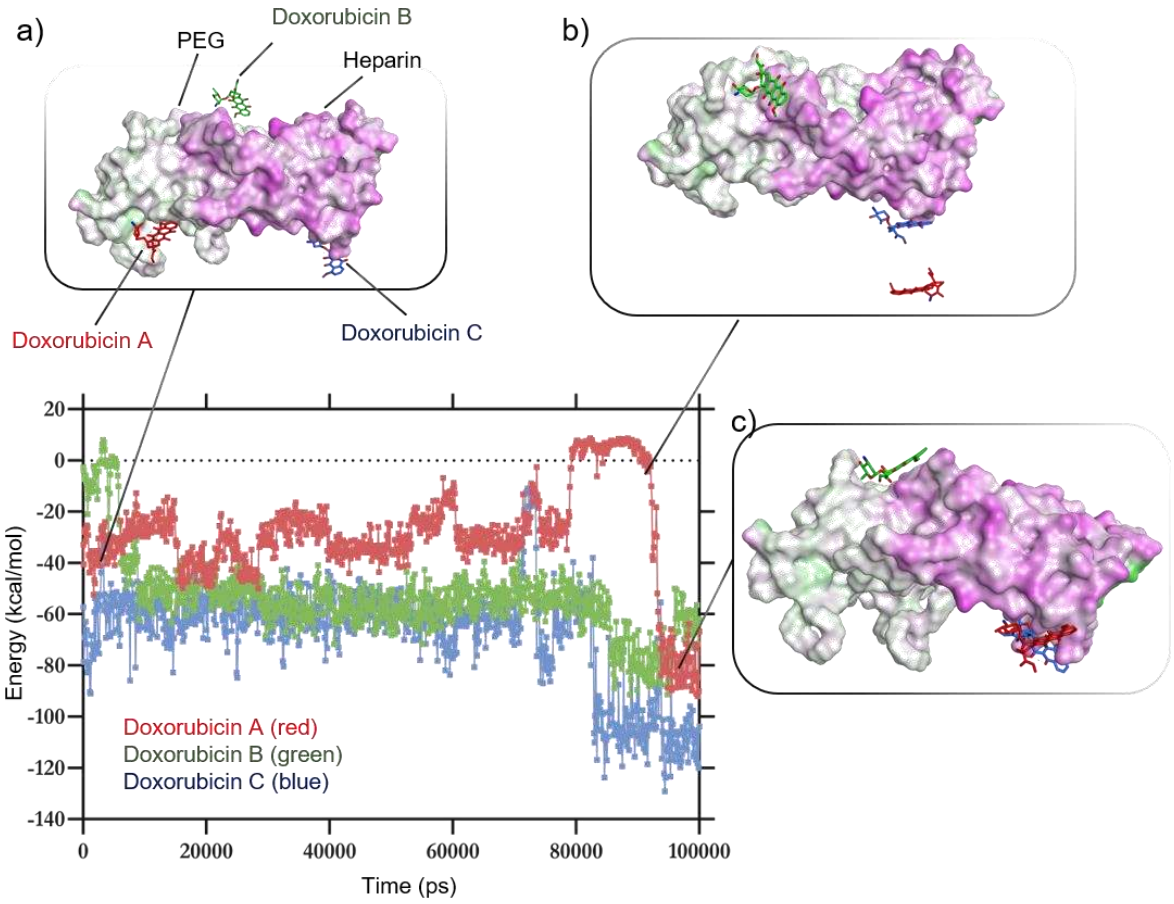

Figure 4. Molecular dynamic simulation of the interaction of three molecules of doxorubicin (A, B and C) with the model PEG/heparin construct to more closely represent the experimental loading condition (standard loading). The starting positions of the doxorubicin molecules were as follows: molecule A near the PEG region, molecule B in the water near the PEG/heparin border, molecule C near the heparin region. (a) The position of the three doxorubicin molecules near the beginning of the simulation. (b) The least stable conformation of the system – during transit of doxorubicin A to the heparin region. (c) The conformation of the most stable (i.e. lowest total energy) of the 100 ns simulation. Note that although doxorubicin A appears in close proximity to doxorubicin C, no π- π stacking is apparent at this stage (see Supplementary Video S2 for full simulation).

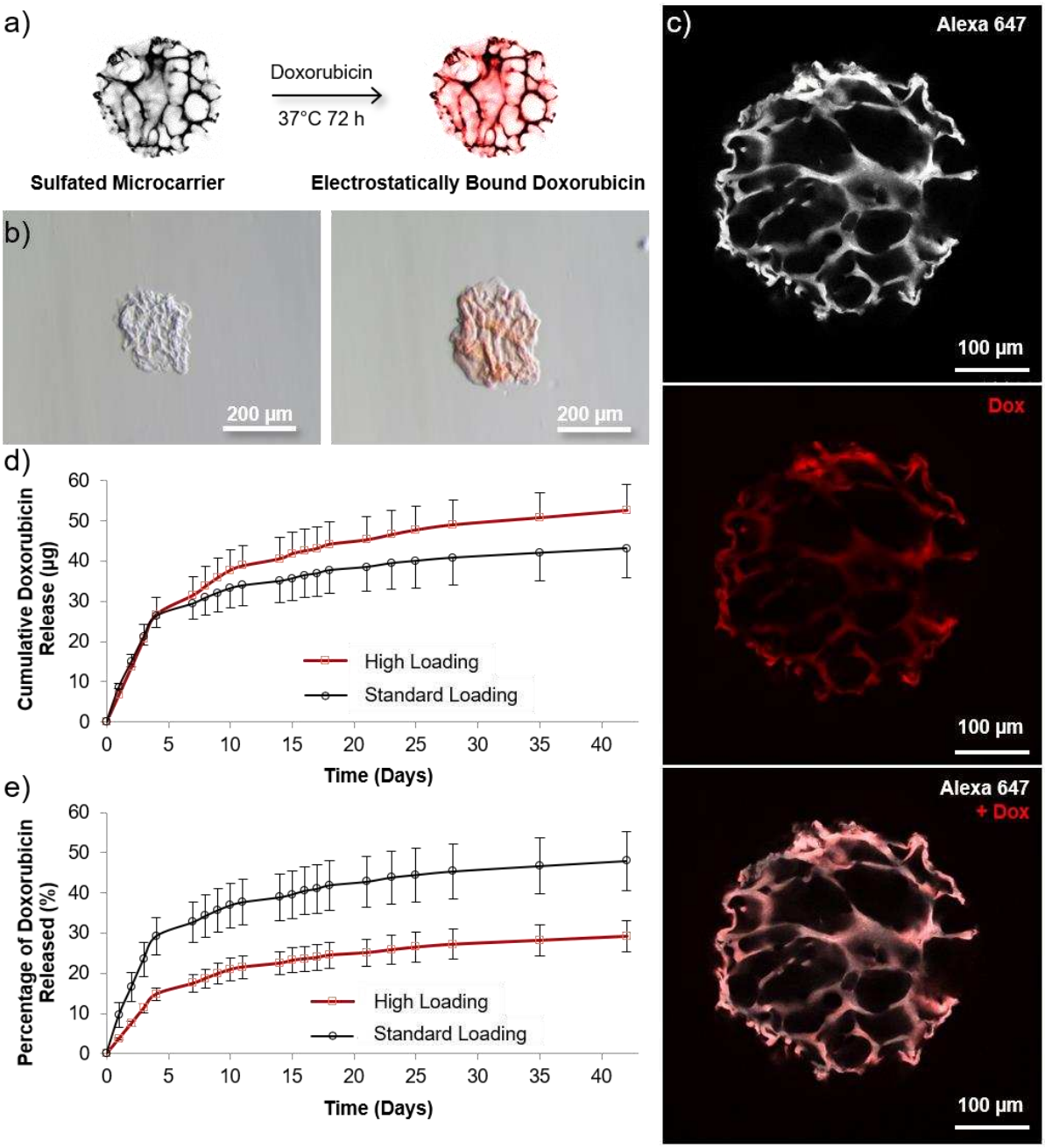

Figure 5. Heparin-based microcarriers load doxorubicin and release it in a controlled manner over an extended timeframe without a burst release. (a) A schematic depiction on the loading conditions used for electrostatic binding of doxorubicin to the heparin component of the microcarriers. (b) Brightfield microscopy images of the microcarriers and the subsequent color change upon loading with doxorubicin. (c) Qualitative confocal laser fluorescence microscopy analysis of the doxorubicin loaded microcarriers showing the intrinsic fluorescence of

doxorubicin (red) overlapping with the struts of the microcarrier (white). (d) The cumulative release profile of doxorubicin was measured for microcarriers loaded with two different concentrations of doxorubicin (66.6 μg doxorubicin/mg microcarriers “standard loading” or 133.3 μg doxorubicin/mg microcarriers “high loading”), with the subsequent percentage released shown in panel (e).

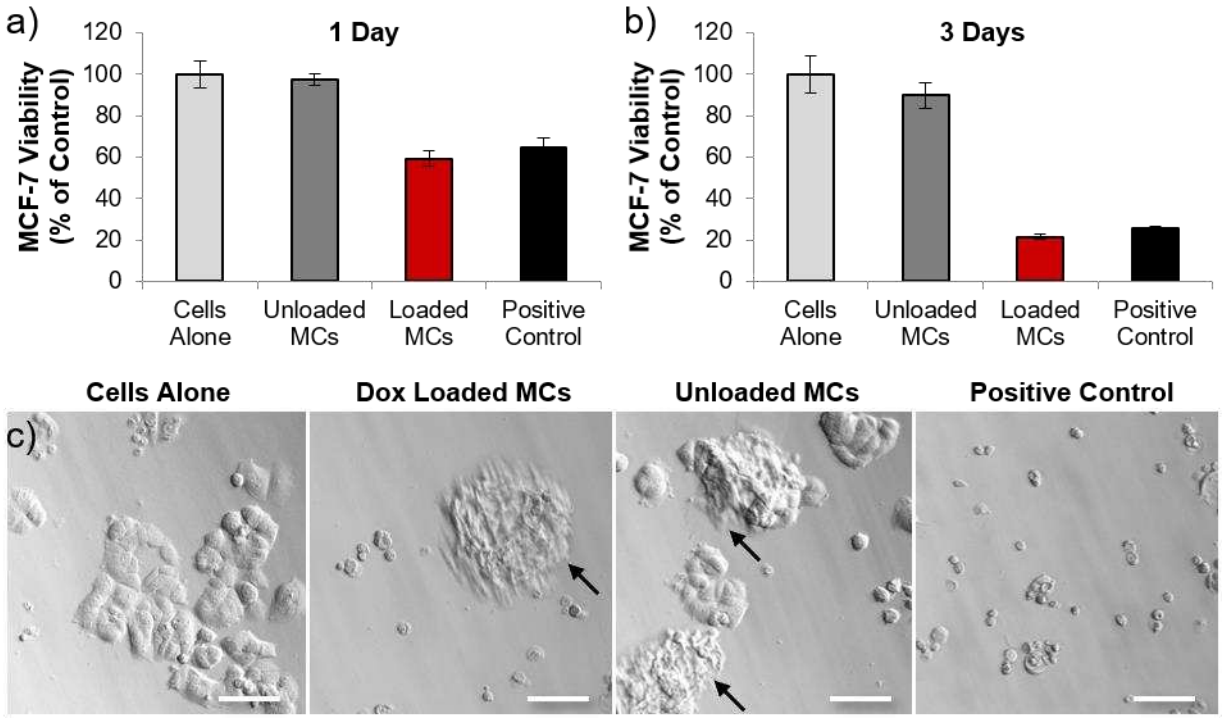

Figure 6. Doxorubicin loaded microcarriers reduce the viability of MCF-7 breast cancer cells *in vitro*. Microcarriers loaded with 40 µg doxorubicin/mg of microcarrier caused a reduction in MCF-7 viability after (a) 1 day and (b) 3 days of incubation. Unloaded microcarriers caused no loss in cell viability. Doxorubicin at a concentration of 4 µg/mL in medium was used as a positive control (n=4). (c) Representative brightfield images of the MCF-7 cells after 3 days in culture. Black arrows indicate microcarriers (out of focus as above the plane of the cells). Scale bars: 100 µm.

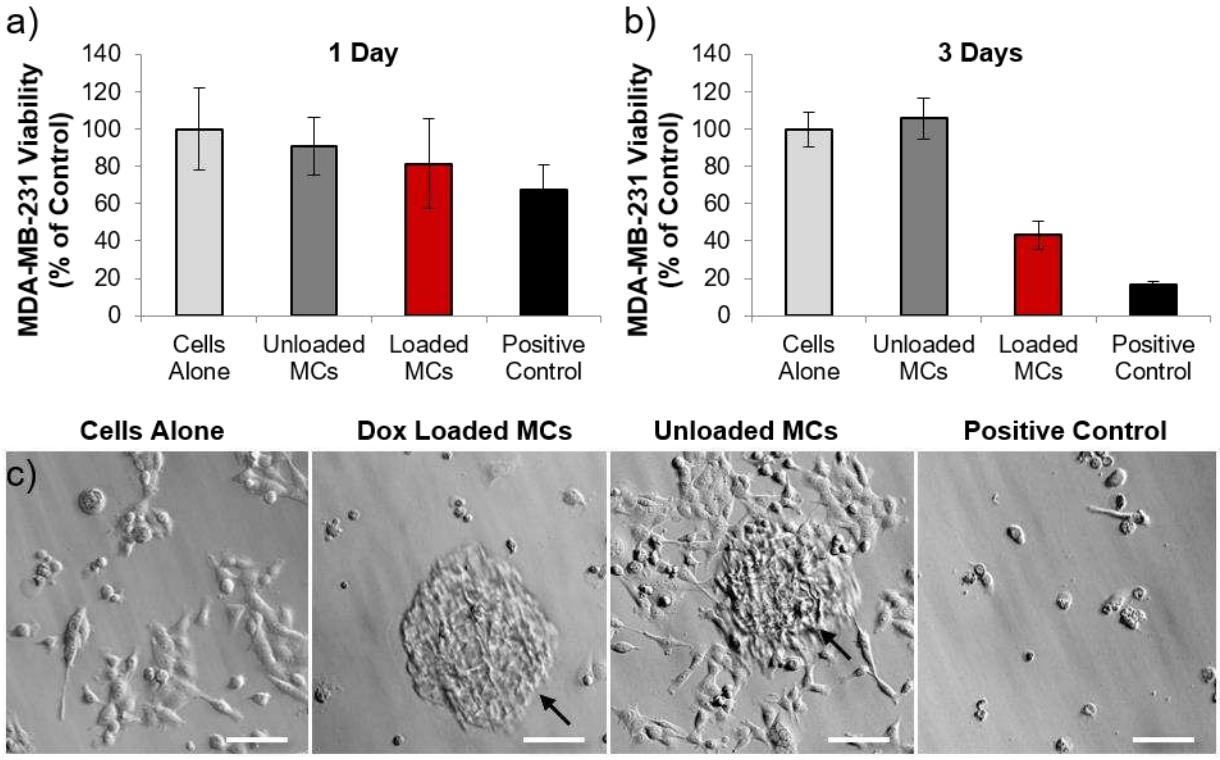

Figure 7. Doxorubicin-loaded microcarriers reduce the viability of triple negative MDA-MB-231 breast cancer cells *in vitro*. Microcarriers loaded with 40 µg doxorubicin/mg of microcarrier caused very little reduction in cell viability after 1 day of incubation (a), but a decrease in viability was observed after 3 days of incubation (b). Unloaded microcarriers caused no loss of cell viability. Doxorubicin at a concentration of 4 µg/mL was used as a positive control (n=4). (c) Representative brightfield images of the MDA-MB-231 cells after three days in culture. Black arrows indicate microcarriers (out of focus as above the plane of the cells). Scale bars: 100 µm.

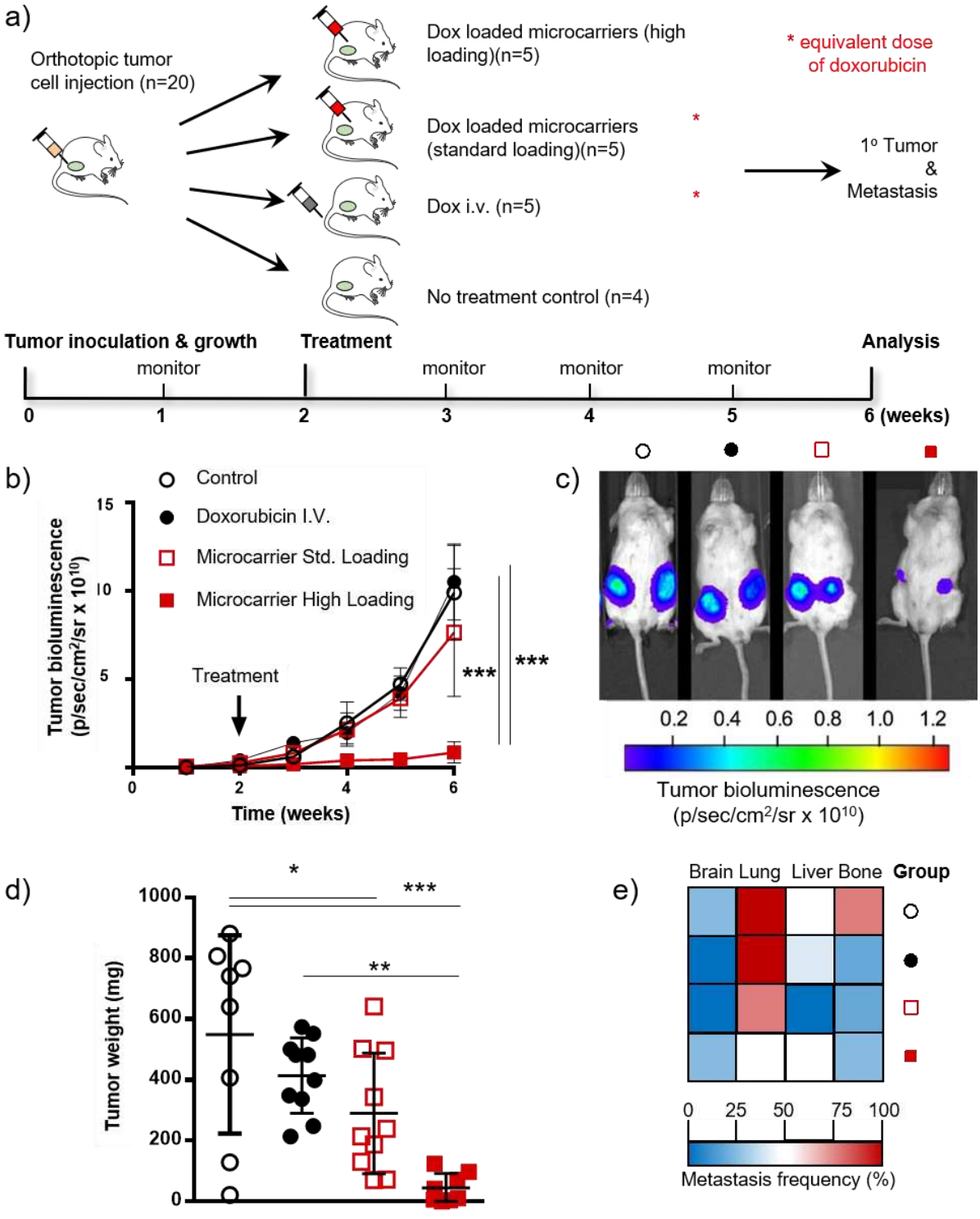

Figure 8. Doxorubicin loaded microcarriers reduce orthotopic breast cancer growth, tumor weight and metastasis *in vivo*. (a) Schematic of the experimental approach. (b) Treatment of

tumor-bearing mice either with doxorubicin-loaded microcarriers (80 μg doxorubicin/mouse "standard loading" and 160 μg doxorubicin/mouse "high loading") or doxorubicin (80 μg/mouse) administered by intravenous dosing. Tumor growth was monitored *in vivo* by noninvasive, cancer cell-specific bioluminescence imaging (two-way ANOVA). (c) Representative bioluminescence composite image at week 6. (d) Primary tumor weights were assessed at the end of the study (week 6) (one-way ANOVA). (e) Heat map of metastatic spread of cancer cells to organs at week 6. Error bars are hidden in the plot-symbol when not visible, n=5 for the high loading microcarrier group (week 1 to 3) and then n = 4 for rest of study. Statistical difference is indicated in comparison to control groups where $*P < .05$, $**P < .01$, and $***P < 0.001$.

Graphical Abstract

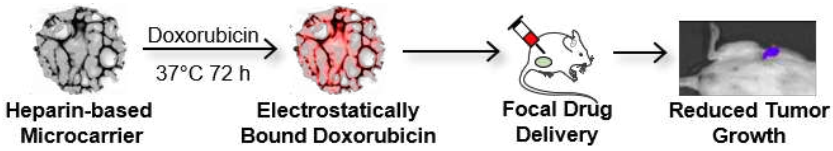

Supplementary Information

Focal drug administration via heparin-containing cryogel microcarriers reduces cancer growth and metastasis

Ben Newland, Carmine Varricchio, Yvonne Körner, Franziska Hoppe, Christian Taplan, Heike Newland, Dimitri Eigel, G. Tornillo, Dagmar Pette, Andrea Brancale, Petra B. Welzel, F. Philipp Seib, Carsten Werner*

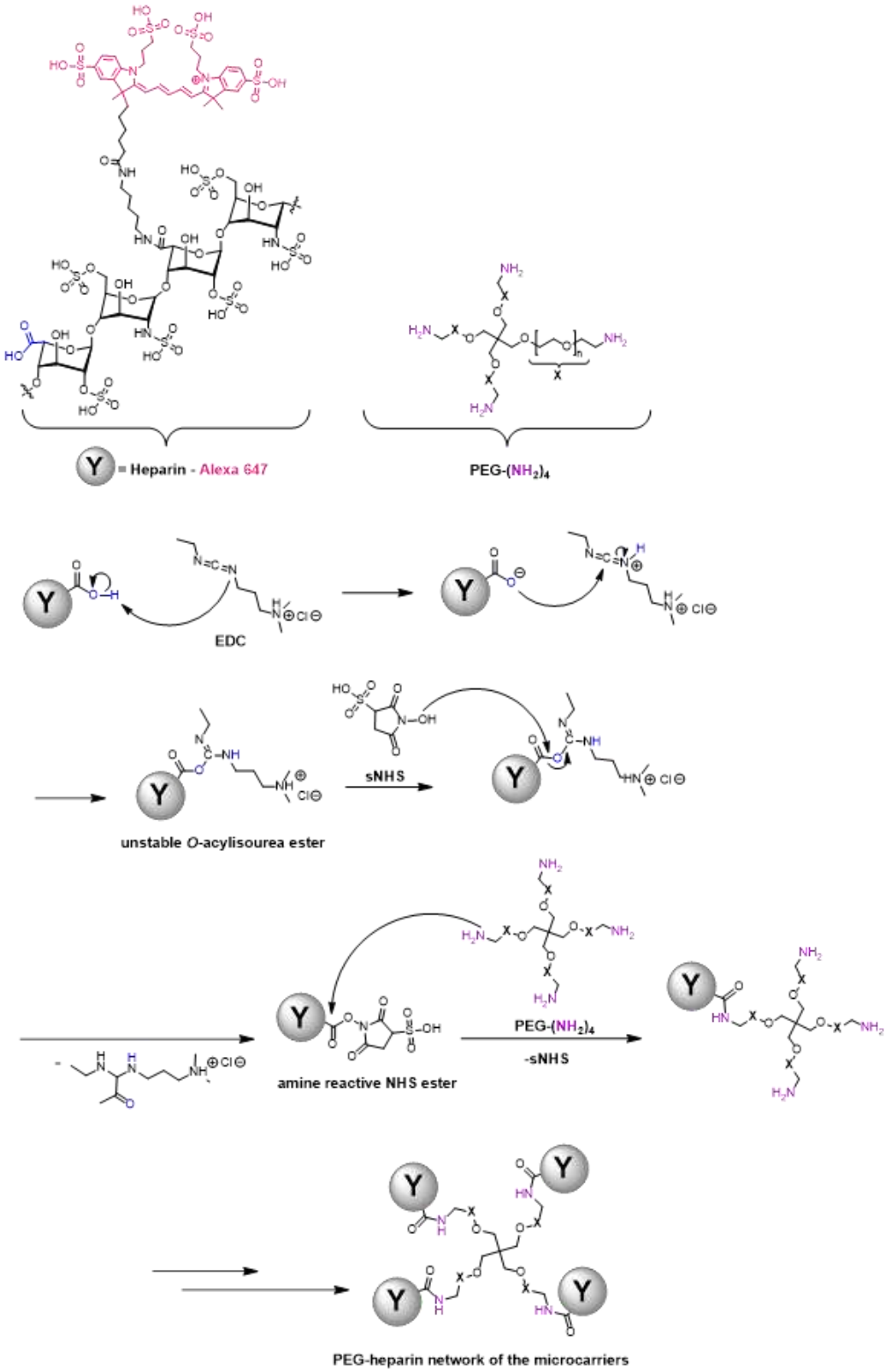

Figure S1. A graphic depiction of the reaction mechanism for microcarriers synthesis from poly(ethylene glycol) and heparin.

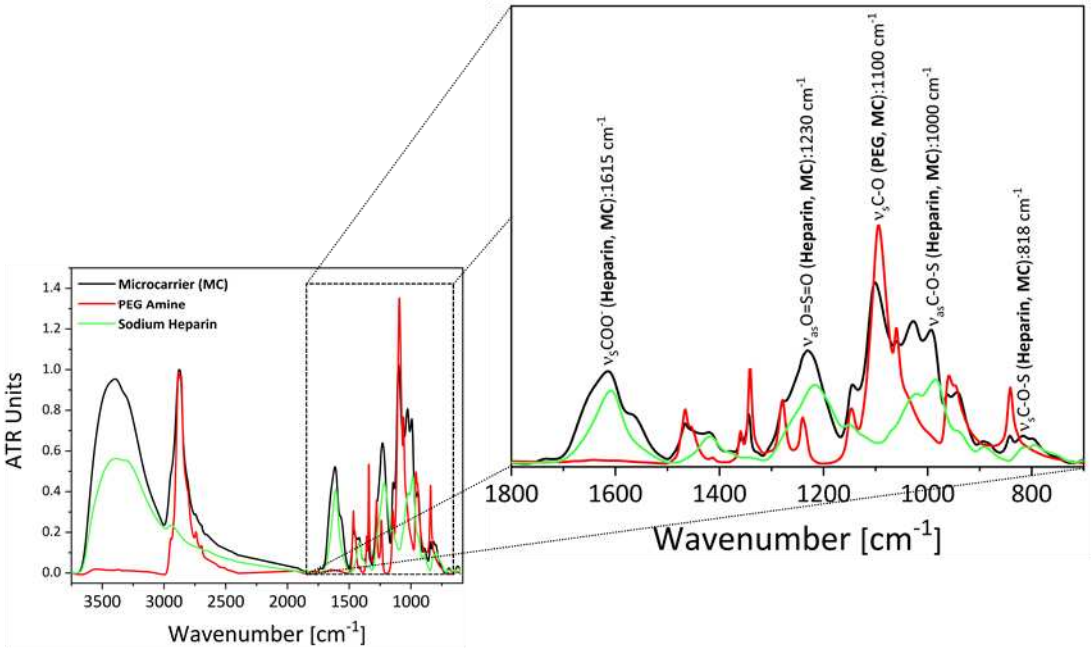

Figure S2. Fourier-transform infrared (FTIR) spectroscopy analysis of heparin, PEG and the PEG/heparin microcarriers proving incorporation of heparin into the microcarrier structure.

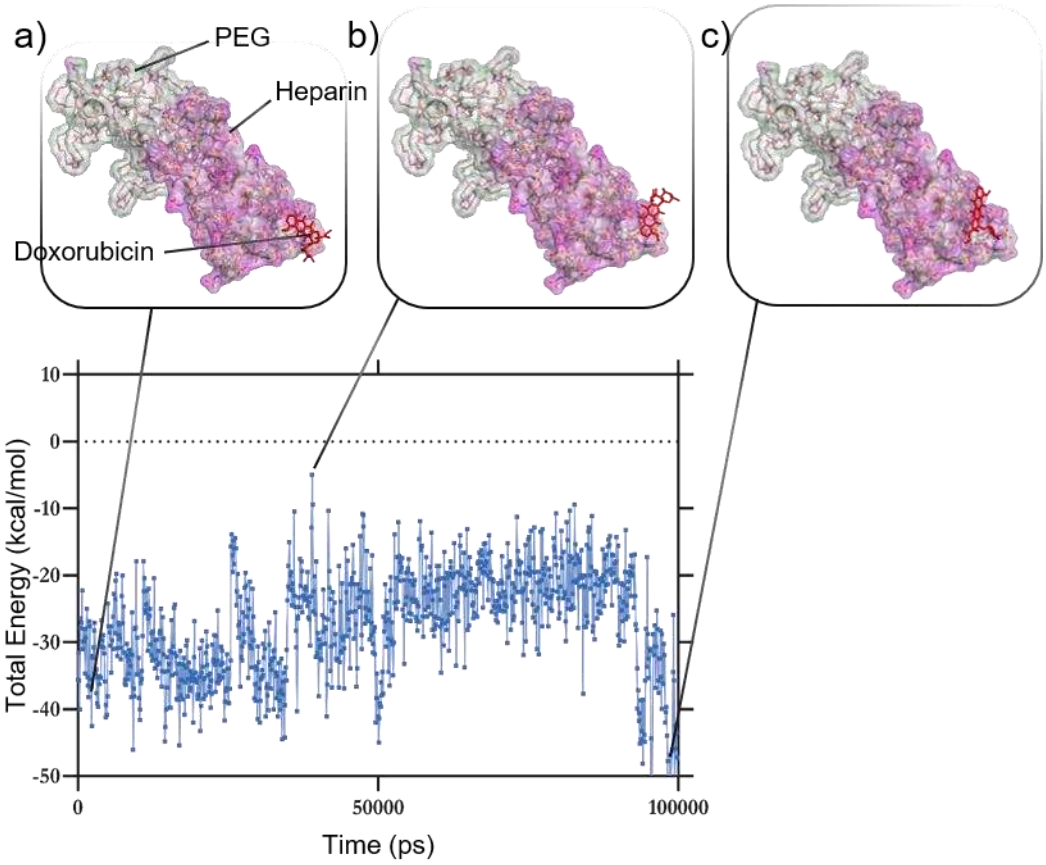

Figure S3. Molecular dynamic simulation of the interaction of doxorubicin with the model PEG/heparin construct, **with an initial doxorubicin position near the heparin region**. The graph shows the variations of total energy of the system during the simulation. The three images (a-c) show the molecular structures at different states of the system during the simulation: a) the position and orientation of doxorubicin at time 0 (starting point), with little change in position (b) until the system energy is at its minimum (i.e. the most stable condition) (c). This simulation clearly shows that doxorubicin remains bound to the heparin region of the model construct rather than moving to the PEG region (see supplementary video S3 for full simulation).

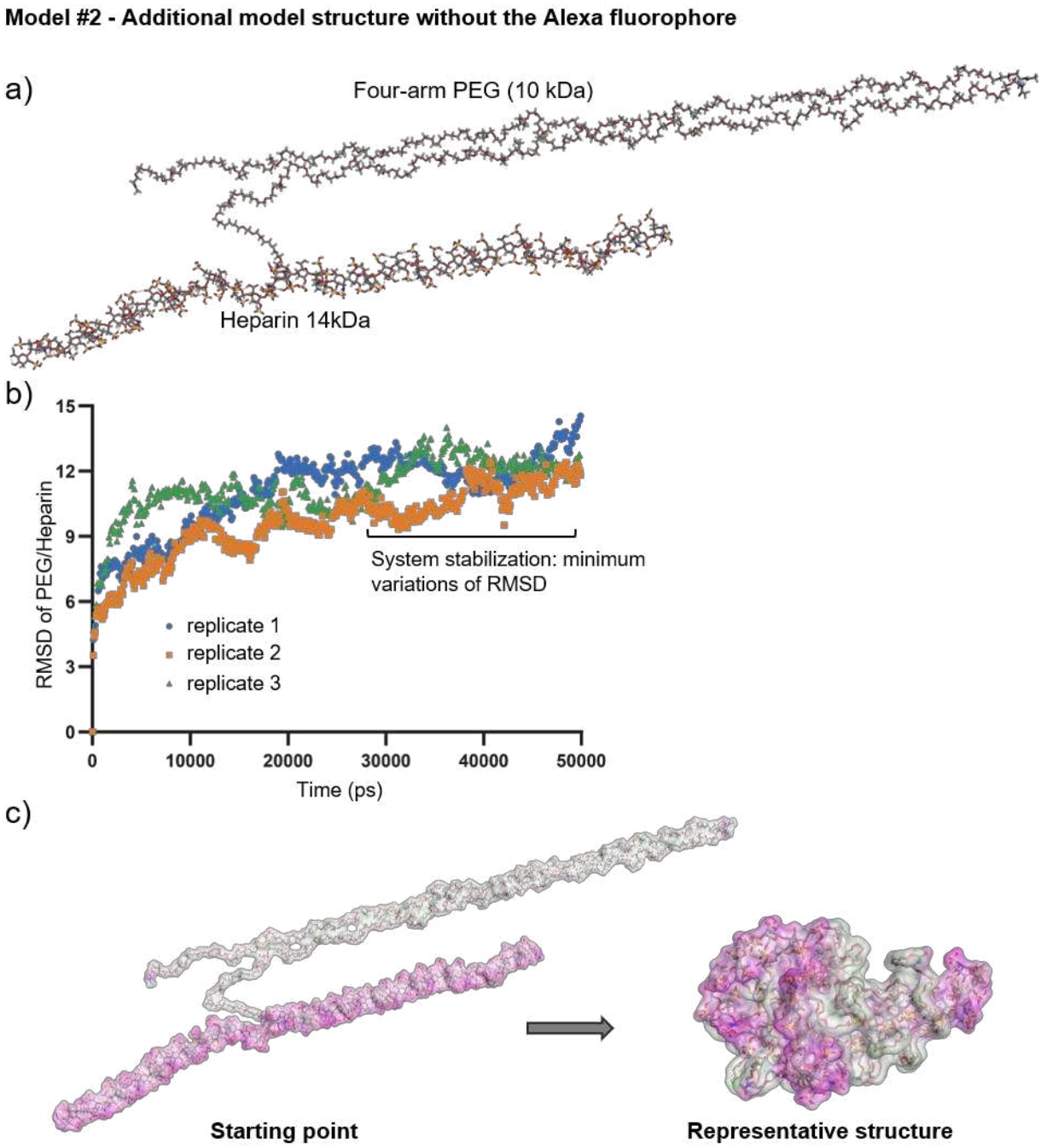

Figure S4. A second PEG/heparin model construct for molecular dynamic simulations but without the fluorophore: (a) Molecular structure of the model PEG/heparin construct created from one PEG molecule and one heparin molecule (i.e. the same molar ratio as used for microcarrier preparation). (b) Graph showing the root-mean-squared distance (RMSD) vs time for the model PEG/heparin construct in water (n=3), from which the representative folded structure (used for subsequent computational analyses) was derived, shown rendered in (c).

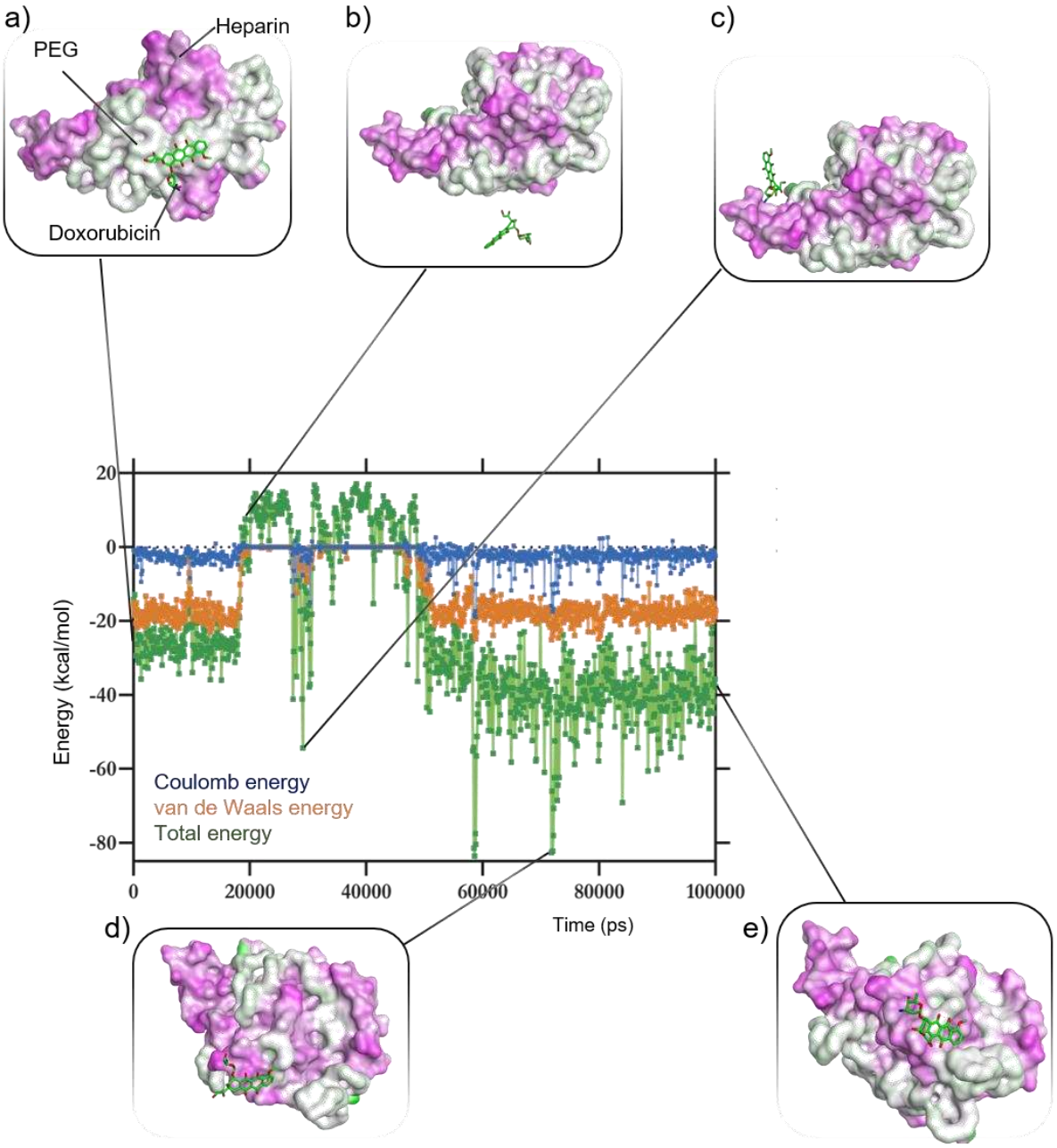

Figure S5. Molecular dynamic simulation of the interaction of doxorubicin with the second model PEG/heparin construct (without fluorophore). The graph shows the variations of total energy of the system during the simulation (system contains one doxorubicin molecule and one model PEG/heparin construct). The four images show the molecular structures in different states of the system during the simulation. (a) The position and orientation of doxorubicin at time 0 (starting point) placed near the PEG region of the model construct. (b) The doxorubicin position when the total energy is the highest (in the surrounding water). (c) The initial interaction of doxorubicin with the heparin part of the model PEG/heparin construct. (d) The situation where the system energy is at its minimum (i.e. the most stable condition). This simulation clearly shows preferential binding of doxorubicin to the heparin region rather than the PEG region of the construct (see supplementary video S4 for full simulation).

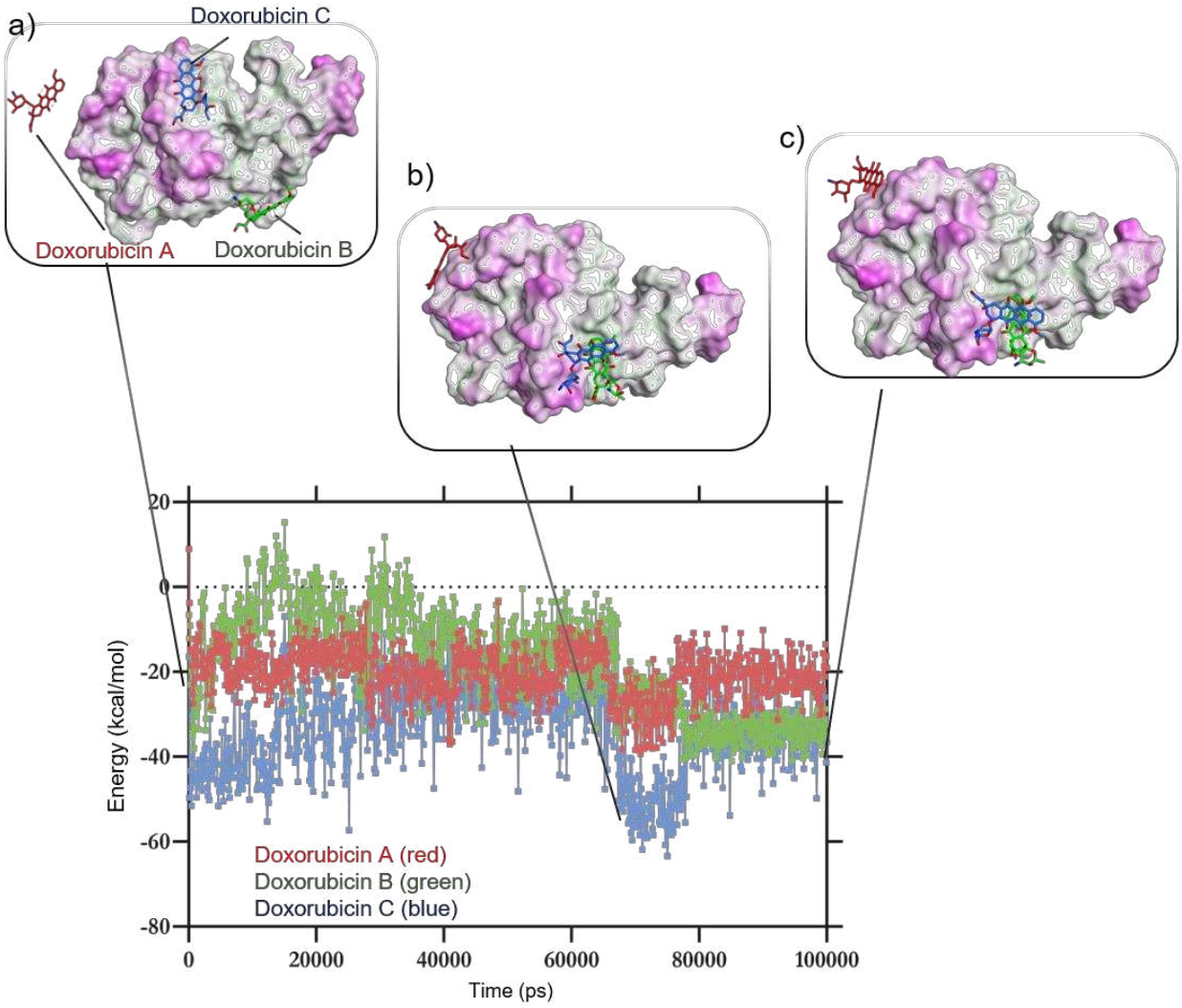

Figure S6. Molecular dynamic simulation of the interaction of three molecules of doxorubicin with the second model PEG/heparin construct (i.e. without fluorophore) to more closely represent the experimental loading condition. The starting positions of the doxorubicin molecules were as follows: molecule A near the PEG region, molecule B in the water near the PEG/heparin border, molecule C near the heparin region. (a) Shows the position of the three doxorubicin molecules near the beginning of the simulation. (b) Shows the least stable conformation of the system – during transit of doxorubicin A to the heparin region. (c) The conformation of the most stable (lowest total energy) of the 100 ns simulation – note that although doxorubicin A appears in close proximity to doxorubicin C, there does not appear to be any π- π stacking at this stage (see Supplementary Video S5 for full simulation).

a)

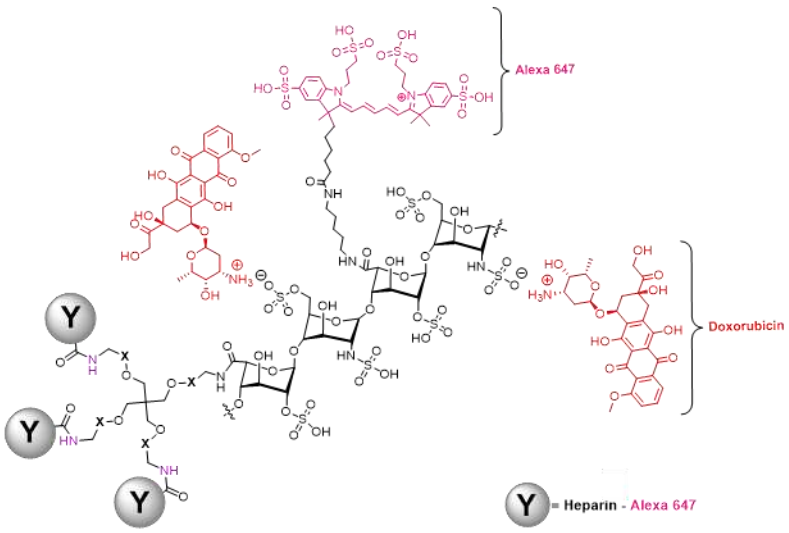

b)

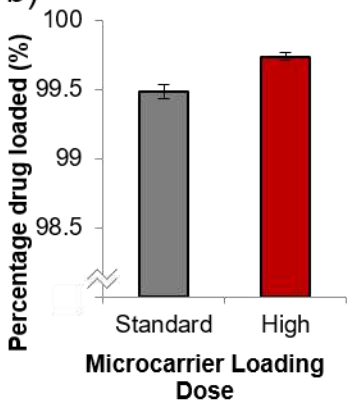

c)

	Heparin	Doxorubicin (Std)	Doxorubcin (high)
M (g/mol)	14000	579.98	
Mass used (µg)	583.3	66.6	133.3
Amount (µmol)	0.042	0.115	0.230
Amount of SO_4 groups (µmol)	2.7		
Dox/heparin ratio		2.76	5.52
Dox/SO_4 group ratio		0.043	0.085

Figure S7 – (a) Proposed interaction of doxorubicin with the sulfate groups of microcarriers. (b) Analysis of the uptake of doxorubicin to the microcarriers at either 66.6 µg dox/mg MC "standard loading" or 133.3 µg dox/mg MC "high loading (n=3, error bars represent ± standard deviation). (c) Table of values used to calculate the drug/heparin or drug to sulfate group ratio, when 1 mg of microcarriers are loaded with either 66.6 or 133.3 µg of doxorubicin.

Table S1 – Analysis of RMSD, van der Waals energy, Coulomb's energy and total energy throughout the simulation trajectory described in Figure 3 and Supplementary Information Video S1.

Time steps	RMSD (Å)		Coulomb's energy (kcal/mol)		vdW energy (kcal/mol)		Total energy (kcal/mol)	
(ns)	Range	difference	range	mean	range	mean	range	mean
0-10	2.07 to 0	2.07	1.64 to -8.34	-0.74	-3.63 to -25.68	-13.93	-3.66 to -30.11	-15.58
10-20	11.80 to 1.84	9.96	0.92 to -3.01	-0.08	0 to -16.32	-2.01	-3.12 to -20.83	-2.34
20-30	10.50 to 7.57	2.93	- 0.15 to -16.82	-7.50	-7.77 to -27.95	-15.81	-9.36 to -29.97	-21.47
30-40	10.75 to 7.95	3.18	-1.37 to -14.58	-6.77	-6.92 to -27.58	-16.57	-11.49 to -33.92	-21.98
40-50	10.58 to 7.76	2.82	1.20 to -13.72	-5.11	-4.58 to -29.07	-17.92	-4.27 to -40.89	-26.65

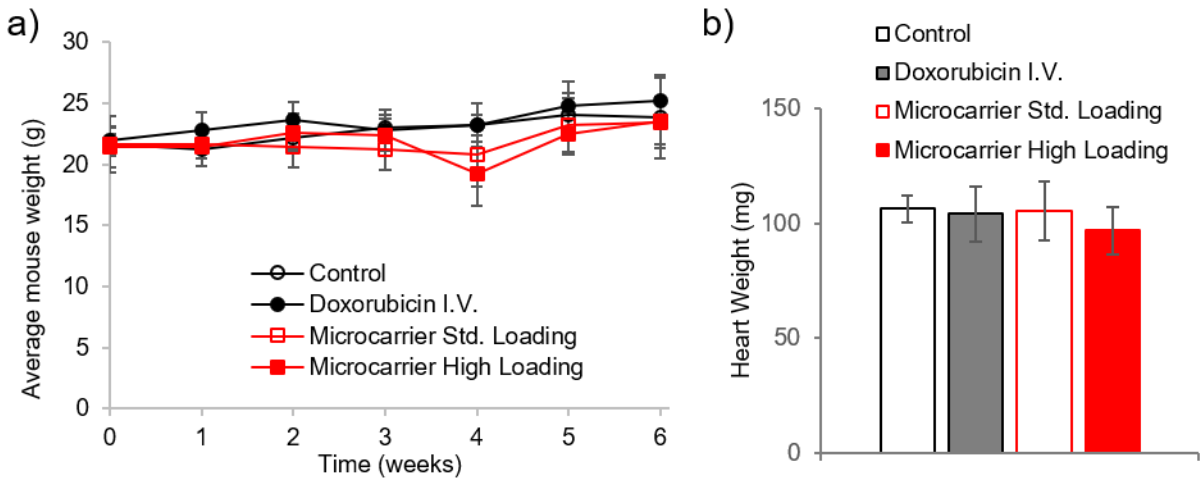

Figure S8. Mouse weight (a) and heart weight (b) were not affected by the administration of the microcarriers (error bars represent ± standard deviation, no significant difference between groups was shown (one-way ANOVA with Tukey's multiple comparison test where a *P*-value ≤ .05 was considered a statistically significant difference)).